LIST OF TABLES

TABLE OF CONTENTS

ACKNOWLEDGMENTS

I would like to thank my principal supervisor Johan Kruger, and other supervisors, Craig Smith and Ray Durrheim. Thanks also go to the staff of the Bernard Price Institute Isotopes Group, Erika Barton, Mike Duane, Alistair Moyes, Ingeborg Swinley, Joe Aphane, Esi Mathlaku, Trevor Clark, Janet Moyes, Sonja Reid and Fatima Variava for their advice and guidance in this research, and their assistance in dealing with the university administration. Thanks also go to Mike Jones, Tomas Wallmach, and Grant Cawthorn for the assistance given in the course of the project.

Mark Bristow of Rand Mines and the staff of Winterveld Chrome Mine and Crocodile River Platinum mine are also thanked for the help given in sampling, as is Rev. Jerry Dibetso of the Lutheran Church in Jane Furse, for providing accommodation during a field trip to Sekhukhuneland.

Thanks also go to the Geological Survey, especially Edgar Stettler and the staff of the library for allowing me the opportunity to complete this dissertation and for making facilities available.

DECLARATION

I declare that this dissertation is my own, unaided work. It is being submitted for the degree of Master of Science in the University of the Witwatersrand, Johannesburg. It has not been submitted for any degree or examination in any other university.

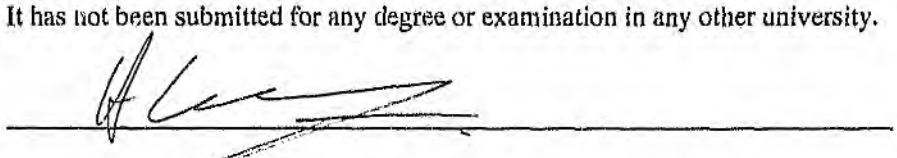

16 day of November, 19 95

Rb-Sr data from garnets and their pelitic matrix from the contact aureole of the Bushveld Complex indicate an extended period of cooling, with at least 13 Ma between the intrusion and the final closure of the garnets. A geothermometric study on these garnets indicates a temperature of 586°C at the end of garnet growth.

The Bushveld Complex is therefore the result of a prolonged thermal event, including the intrusive event which lasted less than 4 Ma and an immediate post-emplacement hydrothermal alteration phase with a duration of at least 13 Ma. This indicates a period of elevated heat flow in the Kaapvaal Craton *c.*2 Ga years ago, most likely related to the Kheis orogeny.

ABSTRACT

Detailed high precision geochronological studies have been performed on the 2054 Ma old Bushveld Complex, in an attempt to unravel its tectonic and thermal evolution in the period immediately following intrusion and crystallisation. The geochronological techniques used have been specifically chosen to sample specific temperature episodes in the cooling of the Complex, rather than to necessarily provide an accurate emplacement age. The Bushveld Complex is seen in this study as part of the Bushveld Magmatic Province, rather than as an isolated intrusion. The geochronological data are therefore interpreted in the context of the current understanding o . the Proterozoic tectonic and thermal history of the Kaapvaal Craton.

The development of clean chemical methods and accurate geochronological methods are essential to this type of study. The reduction of laboratory blanks, especially for lead and the development of laboratory techniques for the analysis of small samples therefore played an important part in this study. It has been possible to lower analytical blanks, especially lead blanks to levels where the analysis of small samples is possible. In addition, the zircon evaporation technique was attempted.

Phlogopite micas from the Critical Zone of the Bushveld Complex give a wide range of Rb-Sr model ages, some almost 100Ma older than the preferred age. This indicates a period of hydrothermal alteration of considerable duration at the same time as the intrusion. The slightly young Rb-Sr age recorded for all the mica and whole rock data collected for this study indicates the alteration of the micas which is evident from petrographic and electron microprobe studies.

U-Pb and Pb-Pb zircon ages are also significantly younger than the preferred age, indicating a degree of alteration. This is also seen in the discordance of the zircons seen in the U-Pb data.

THE TECTONO-CHRONOLOGICAL EVOLUTION OF THE BUSHVELD COMPLEX

Hendrik Coetzee

A dissertation submitted to the Faculty of Science of
the University of the Witwatersrand for the degree of
Master of Science

March, 1995

metamorphism, especially of the Venters lorp Sequence, shown by the resetting of the Pb-Pb and Rb-Sr systematics of the Zoetlief Group (Walraven *et al.*, 1991).

These published and unpublished age determinations are adequate for most purposes as they accurately locate the intrusion of the Bushveld Complex in the temporal development of the Kaapvaal Craton, and present a number of ages as which may be physical manifestations of a generally raised geothermal effect, possibly related to the Kheis Orogeny as suggested by Duane and Kruger (*op. cit.*). However, the existing geochronological data do not give us any detailed information about the cooling history of the Bushveld Complex or the overall thermal history of this part of the Kaapvaal Craton.

1.3.2 Tectonics, and the incremental development of the Bushveld Complex.

The Bushveld Complex has been shown to be the result of several injections of magma (Hamilton, 1977; Kruger & Marsh, 1982; Sharpe, 1985; Kruger *et al.*,1987; Cawthorn *et al.*, 1991; Davies & Cawthorn, 1984). This indicates that the view of the intrusion of the Bushveld Complex as one single event is not absolutely correct, and may for some purposes be inadequate. The actual cooling of the mafic rocks of the Bushveld Complex to the solidus was however extremely rapid, having taken considerably less than the 2 Ma time constraint indicated by the new zircon data. Walraven (*op. cit.*) and Irvine (*op. cit.*) have calculated the cooling time to the solidus at less than half a million years. Nevertheless, in modern day plate tectonic terms, the period of development of the Bushveld Complex after cooling below the solidus may span periods where significant plate movements took place. The long cooling indicated by some of the "young" (for example Kruger and Onstott's unpublished 2010 Ma $^{40}Ar/^{39}Ar$ age) ages for the Bushveld could indicate anomalously high temperatures for several tens of millions of years after intrusion. Taking modern plate velocities into account, this period could translate to as much as 6000km of plate movement. Nevertheless, the relatively consistent palaeopole (Layer *op. cit.*, Hattingh, 1986a,b,c, Gough & van Niekerk. 1959) indicates fairly restricted movement. This suggests

The other units which constrain the absolute age of the Bushveld rocks are the older Pretoria Group, dated at 2224±21 Ma (Burger & Coertze, 1973, quoted in Walraven *et al., op. cit.*) and the younger Vredefort event, which has been dated at 2002±52 Ma (Compston & Nicolaysen (unpubl. ion-microprobe data) , quoted in Walraven *et al., op. cit.*).

Coetzee & Kruger (*op. cit.*) report an age of 2041±41 Ma for the Losberg Complex which is indistinguishable from that of the Bushveld Complex. Similarly the Molopo Farms Complex appears to be of the same origin as the Bushveld Complex (C. Lee, pers. comm., Kruger, unpubl. data). Coetzee & Kruger (*op. cit.*) therefore assign all these intrusions to a single widespread magmatic event, the Bushveld Magmatic Province.

All these data point only to a 2054 Ma intrusive age for the Bushveld Complex and not to any incremental development. Irvine (*op. cit.*) and Walraven (1981) have however placed a constraint on the solidification time of the layered rocks, estimating this to be between 200 000 and 350 000 years. These determinations are in agreement with the <1 Ma interval between the intrusion of the Critical and Upper Zones reported by Armstrong.

Contemporaneous with the intrusion of the Bushveld Complex, other important geological processes were occurring on the Kaapvaal Craton. The *c.* 2.05 Ga Phalaborwa Complex was intruded (Erikson, 1984) and the Kheis orogeny occurred in the *c.* 1.9-2.1 Ma time frame (Duane & Kruger, *op. cit.*). These data, the *c.* 2.0 Ga metamorphic overprint recorded in the Onverwacht cherts in the Barberton area (Weis & Wasserburg, 1987) and the evidence of palaeomagnetic realignment of shales from the Witwatersrand Supergroup to a 1950-2050 Ma palaeopole (Layer *et al.*, 1988) point towards a major thermal event in the craton contemporaneous with the intrusion of the Bushveld Complex. Duane & Kruger (*op. cit.*) believe that hot fluids driven east during the Kheis Orogeny were partly responsible for this resetting and

to construct a thermal chronology for the Bushveld Complex. This includes an investigation of the temporal and genetic relationships between the different manifestations of the c. 2 Ga Bushveld Magmatic Province of the Kaapvaal Craton.

1.3 Review

1.3.1 Geochronology

The first age determinations performed on rocks from the Bushveld Magmatic Province were those of Schreiner (1958) and Nicolaysen *et al.* (1958). They calculated ages of *c.* 1900 Ma for the Bushveld Granite and 2006±50 Ma for the Bushveld Complex respectively. Subsequent workers have almost all determined ages in the range 1.9-2.1 Ga (Walraven *et al.*, 1990). Walraven *et al.* (*op. cit.*) have compiled a review of geochronological data for the north-central Kaapvaal Craton, where they present preferred ages of 2061±27 Ma for the layered rocks and 2052±48 Ma for the granitic rocks.

Recently Armstrong (pers. comm., 1993) has determined a U-Pb single zircon age for the mafic rocks of the Bushveld Complex of 2054±1 Ma. This age has been repeated with zircons from the Critical and Upper Zones, and can therefore also be used to constrain the intrusive history of the complex. Walraven and Hattingh (1993) have dated the Nebo Granite at 2054.4±1.8 Ma using the zircon evaporation technique. These two results are indistinguishable at the 2σ level (±1.8 Ma). This important result shows that the two intrusive events occurred almost simultaneously and are therefore probably related. In this study, the age given for the Nebo Granite is taken as the best available age, and provides a minimum age for the mafic rocks. There are few dates for events on the cooling curve of the complex, although Onstott and Kruger have determined a 2010±10 Ma age for a temperature of 400°C, using the Ar-Ar method on mica (pers. comm., F J Kruger).

1.2 Aims of this study

This study aims to piece together the early post emplacement chronology of the Bushveld Complex. The preferred age of c.2.05-2.06 Ga is adequate for the more usual purpose of situating the rocks within the chronostratigraphy of the Kaapvaal Craton. However, it does not have the necessary precision for detailed tectonic and petrological modelling, nor does it provide any information about the incremental development of the complex.

The geochronometric methods used in this study aim to sample the cooling curves of these rocks, the different minerals and isotopic systems employed becoming blocked at specific temperatures and times. Similarly, the magnetic minerals in rocks acquire a remanent magnetisation at a specific blocking temperature and also record the structural attitude of the rocks at that time. It should therefore be possible to construct a time-temperature-structural curve for the thermal evolution of an igneous body using isotopic, thermometric and palaeomagnetic data and thereby constrain the rate at which thermal and tectonic processes occurred. The metamorphic rocks surrounding an igneous intrusion can be used as geothermometers, geobarometers and geochronometers for the igneous rocks. Where it is possible to discern the incremental growth of metamorphic minerals, they can be used to determine the thermal development of the environment in which growth took place.

This type of modelling requires the use of geochronometers which date specific points in the cooling history of the body, and which are precise enough to allow these events to be separated in time. This type of study is particularly useful as it allows us to constrain the duration of tectonic and magmatic processes, on the Kaapvaal Craton during this period of tectonism. Specifically, the isotopic systems which are investigated are the uranium-lead and lead-lead systems in zircons, rubidium-strontium and argon-argon in micas and the strontium isotopic evolution during the growth of garnets in the metamorphic aureole. This work therefore aims to adapt and develop high precision dating techniques on appropriate minerals, and to use these techniques

Biljon, 1949 & 1974). None of these workers attempted to put specific time constraints on the processes that they invoked, except that the orthomagmatists viewed the intrusion as one rapid process, while the transformationists saw the Complex's formation as a somewhat more protracted process.

To date the geological and geochemical work on the Bushveld Complex has been largely concerned with its structure, composition, magma genesis and economic mineralisation. Geochronological studies have been aimed at determining the absolute age of the body. In all these studies, there has been little attention given to the thermal evolution of the body, except by Irvine (1970), Wairaven (1981) and Kruger & Smart (1987), who deal only with selected aspects of the intrusion. A general consensus seems to have emerged that the mafic rocks of the Bushveld Complex result from a series of intrusions of different magmas, which differentiated and crystallised, prior to the intrusion of the Lebowa Granite Suite (SACS, 1980).

The mafic layered part of the Bushveld Complex comprises a sequence of ultramafic to gabbroic rocks, and is inferred to be the result of multiple injections of magma on the basis of geochemical and isotopic work (Cawthorn *et al.*, 1991). The granites intruded some time after these mafic rocks, and are not comagmatic or directly co-eval. In this work, therefore, the Bushveld Complex is not viewed as a single event in time, but rather as the evolution of a thermal high which had a significant duration and craton-wide effects. This *c.*2.05Ga event is manifested in a number of other intrusions, for example The Losberg (Coetzee & Kruger, 1989) and Phalaborwa (Eriksson, 1984) intrusions. Furthermore, a wide ranging thermal event is seen in palaeomagnetic (Layer, *et al.*, 1988) and isotopic (see for example Weis & Wasserburg, 1987) results, which indicate overprinting at this age. Knowledge of the incremental evolution of the Bushveld Complex and its associated rocks is deducible from field and geochemical relationships, but has not been seen in geochronological studies. Currently, knowledge of the tectonic evolution of the complex is limited to structural and palaeomagnetic studies which cannot as yet be set in a quantitative temporal framework.

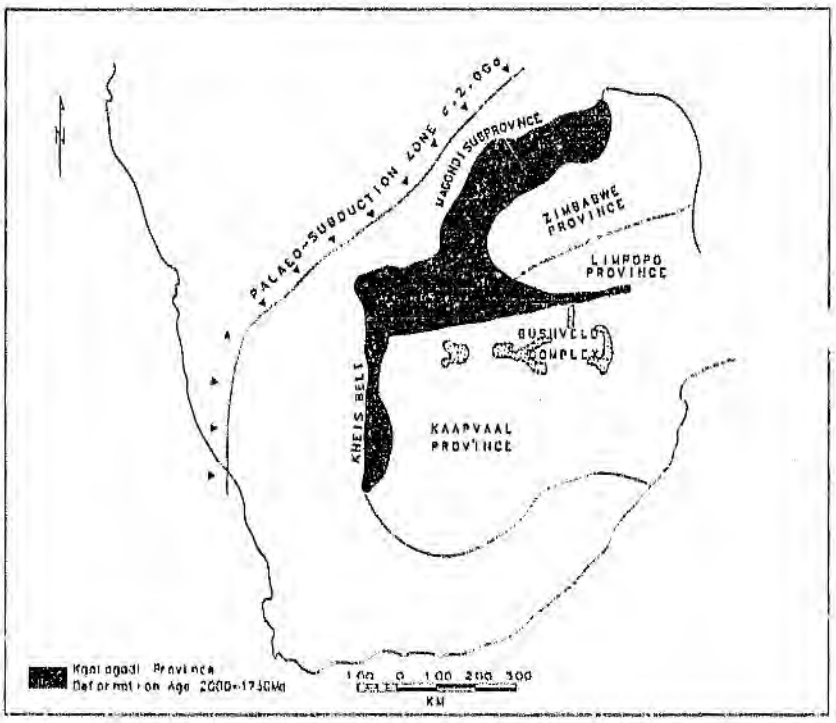

Figure 1.1 Proposed tectonic setting of the Bushveld Complex (After Hartnady *et al.*, 1985)

majority of workers (Molengraaff, *op. cit.*; Hall, 1932; Wagner, 1929; Daly, 1928). Nevertheless, some workers have viewed the rocks as "magmatised" Transvaal sediments transformed by heat and "emanations" (Sandberg, 1926; van

CHAPTER ONE: INTRODUCTION AND REVIEW

1.1 Introduction

The Bushveld Magmatic Province comprises an extensive suite of coeval rocks, intrusive into the Proterozoic Transvaal Sequence and its correlates in Botswana (Coetzee & Kruger, 1989). This Province extends at least from Villa Nora in the north to Losberg in the south, and from Burgersfort in the eastern Transvaal to the Molopo Farms in the west. Gravity Data indicates the presence of dense material (possibly extensions to the Bushveld Complex) to the south east of this area. The Bushveld Complex *per se* covers an area of 65 000km^2. The generally accepted ages for the Bushveld Complex are *c.* 2.06 Ga for the mafic rocks and *c.* 2.05 Ga for the Bushveld Granite.

There is also evidence for widespread metamorphism and tectonism contemporaneous with the intrusion of the Bushveld Complex. (Duane & Kruger, 1991, Coetzee & Kruger, *op. cit.*). Therefore the intrusion of the Bushveld Complex occurred during a period of major tectonism and high heat flow, rather than merely being a single, albeit large magmatic event. (von Gruenewaldt & Harmer, 1992). Figure 1.1 shows the Bushveld Complex in its 2 Ga Kaapvaal Craton tectonic setting.

The Bushveld Complex was first described by Carl Mauch, an explorer and geologist, who travelled in the central and northern Transvaal and Zimbabwe between 1869 and 1872. (Mauch, 1874, Burke, 1969). Mauch mapped a portion of the Bushveld Complex during his expedition to the Blauberg, the Waterberg and the Pilanesberg, in late 1869.

The first detailed study of the intrusion was performed by Molengraaff (1901). Molengraaff and many subsequent workers were concerned with the structure of the body. Important work also exists concerning the nature of the intrusive event or events that produced the complex, which was accepted as being orthomagmatic by the

LIST OF FIGURES AND PLATES

$$\frac{^{207}Pb^*}{^{235}U} = e^{\lambda_{235}t} - 1 \qquad (13)$$

The concordia curve (Wetherill, 1956) is the locus of all points in $^{207}Pb^*/^{235}U$ - $^{206}Pb^*/^{238}U$ space with the same ^{235}U-^{207}Pb and ^{238}U-^{206}Pb ages. Data from pristine samples should plot on this line, and their position on the line indicates the age of the rock. Figure 2.2 shows the Concordia diagram. If in the course of the history of the rock, radiogenic lead has been lost, or uranium gained in a single event (eg. a metamorphic event), any point on the diagram will move along a chord joining its position on concordia to the origin. Subsequent to the episode of lead loss, the point will develop along a curve similar to the concordia, but starting from a new origin. At the present it will lie on a chord joining the crystallisation age and the age of episodic lead loss. This chord is referred to as a discordia curve. Often a suite of cogenetic samples, or mineral grains from a single rock unit will be altered to different degrees, and will define this discordia line, from which the true age of the sample and of the alteration event can be deduced. Examples of concordant and discordant samples are shown on Figure 2.2, together with the effects of uranium loss, uranium gain and lead loss. Lead may be gained during alteration, but the effects will depend on the isotopic composition of the lead gained. This is usually detected by the presence of substantial ^{204}Pb, which is not a daughter of U or Th, but is present in all other natural lead.

The diagram shows the two-point isochrons produced using these data. Note that the slopes of the isochrons in (I) are extremely close together, indicating very small errors in the age, while those for the whole rock sample (ii) show large differences. From these results it can be seen that the model age technique can only be applied to samples with highly radiogenic Sr, unless the initial $^{87}Sr/^{86}Sr$ ratio has been accurately determined.

2.1.4 Uranium-Lead and Lead-geochronology

The uranium-lead system is more complicated than the Rb-Sr system, as it comprises two separate isotopic systems viz:

$^{235}U \rightarrow {}^{207}Pb$

and $^{238}U \rightarrow {}^{206}Pb$

These two isotopes of uranium have different decay constants:

$\lambda_{235} = 9.8485 * 10^{-10} y^{-1}$

$\lambda_{238} = 1.55125 * 10^{-10} y^{-1}$

(Steiger & Jäger, 1977)

Conventional isochron treatment can be used for the two separate isotopic systems, or a number of techniques which include both systems, for example the concordia technique, have been developed.

2.1.4.1 The Concordia diagram

For the U-Pb system, equation 7 can be written as follows.

$$\frac{^{206}Pb^{*}}{^{238}U} = e^{\lambda_{238}t} - 1 \qquad (12)$$

and:

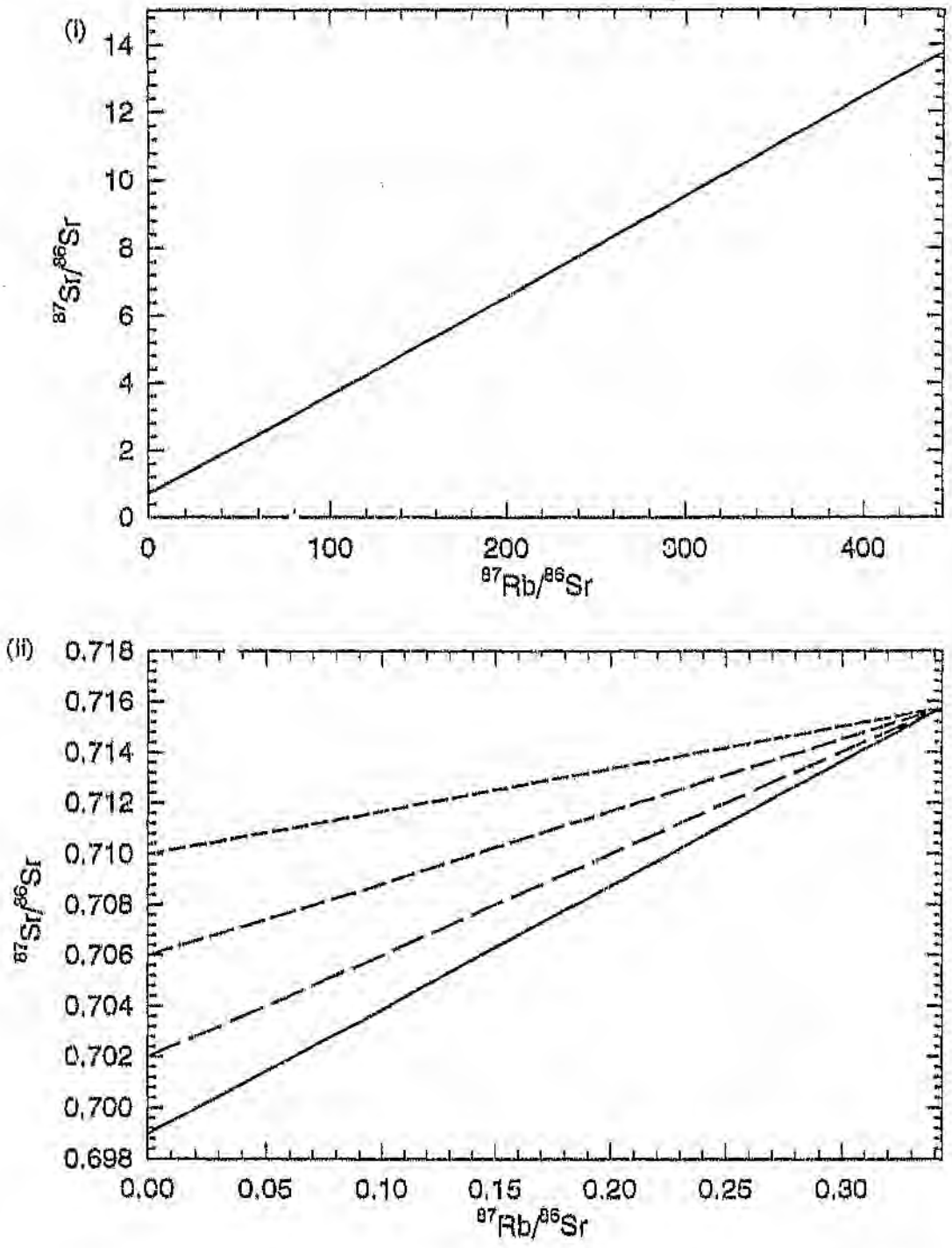

Figure 2.1 Model age isochrons for initial $^{87}Sr/^{86}Sr$ ratios 0.699-0.710 for 2000 Ma samples with (i) high Rb/Sr (eg. micas) and (ii) low Rb/Sr (eg. plagioclase)

accuracy of the model age is dependent on closed system behaviour and the assumption of the correct initial ratio. In some cases, extremely radiogenic $^{87}Sr/^{86}Sr$ ratios are measured. Here, the uncertainty in the age depends more on the uncertainty in the measurement than the initial ratio. In this study, the model age approach is applied to micas from with highly radiogenic $^{87}Sr/^{86}Sr$ ratios. For such samples, the accuracy of the initial ratio chosen for the model age calculation is not particularly important, as shown in the following example.

Model Ages have been calculated for one of the samples in this study, using a range of initial ratios. These are the initial $^{87}Sr/^{86}Sr$ value for the earth, 0.699, calculated from meteorites, 0.702, the ratio for a *c.*2Ga oceanic basalt (Faure, 1986), 0.706, the initial ratio of the Bushveld mafic rocks and 0.715, the initial ratio for the Nebo Granite (Walraven *et al.*, 1990). Within this range, the total variation in age for the sample used is approximately 2 million years, but is dependent on the $^{87}Rb/^{86}Sr$ ratio. It is therefore clear that a small error in the selection of an initial ratio will have little effect on the age calculated using this technique, on samples with highly radiogenic $^{87}Sr/^{86}Sr$ ratios. The data used for this example are presented in table 2.1, and displayed graphically on the isochron diagrams in Figure 2.1.

Table 2.1 Data used to investigate the effect of errors in model ages for P2-biotite and WV3 - whole rock.

Sample	$^{87}Rb/^{86}Sr$	$^{87}Sr/^{86}Sr$	$^{87}Sr/^{86}Sr_i$	Model Age
P2-biotite	443.44	13.767	0.699	2045
P2-biotite	443.44	13.767	0.702	2045
P2-biotite	443.44	13.767	0.706	2044
P2-biotite	443.44	13.767	0.715	2043
WV3 wr	0.3430	0.71576	0.699	4771
WV3 wr	0.3430	0.71576	0.702	2770
WV3 wr	0.3430	0.71576	0.706	1976
WV3 wr	0.3430	0.71576	0.715	5.4

2.1.2 The Isochron diagram

It is generally not possible to assign an exact value to D_0, but this problem can be overcome using an isochron diagram (Nicolaysen *et al.*, 1958). In this method, all of the isotope concentrations referred to in the above equation are expressed relative to an invariant isotope. This also simplifies the analysis, as it is isotopic ratios, and not isotopic concentrations which are measured on the mass spectrometer.

Let the concentration of the invariant isotope of the daughter element be D'. Dividing equation 9 by D' we get:

$$\frac{D}{D'}=\frac{D_0}{D'}+\frac{N}{D'}(e^{\lambda t}-1) \qquad (10)$$

This defines a straight line in N/D' - D/D' space with y-intercept D_0/D' and slope $(e^{\lambda t}-1)$. Therefore if a suite of cogenetic samples is analysed, the age and the isotopic composition of the daughter at time=0 can be calculated. This straight line is referred to as an isochron, a line joining points of equal age (Nicolaysen *et al.*, *op. cit.*).

2.1.3 The Rb-Sr method

The isochron method is used in this study for Rb-Sr dating. For this isotopic system, the isochron equation is written:

$$\frac{^{87}Sr}{^{86}Sr}=(\frac{^{87}Sr}{^{86}Sr})_i+\frac{^{87}Rb}{^{86}Sr}(e^{\lambda t}-1) \qquad (11)$$

where $(^{87}Sr/^{86}Sr)_i$ is the initial Sr isotopic ratio or $_0R$. This equation is explained graphically on Figure 2.1.

Where the initial ratio is known, the slope of the line between the y-intercept point and the point defined by a single analysis may be used to determine the age of the sample. This is known as a model age, as the initial ratio is assumed and not determined. The

This equation gives the number of radioactive parent nuclei which remain after time t, given an initial number N_0 at time t=0.

The number of radiogenic daughter nuclei produced, D^*, is given by:

or:

$$D^* = N_0 - N \qquad (5)$$

$$D^* = N_0(1 - e^{-\lambda t}) \qquad (6)$$

$$D^* = N(e^{\lambda t} - 1) \qquad (7)$$

Since:

$$D = D_0 + D^* \qquad (8)$$

where: D^* is the number of daughter nuclei produced in time t,

D_0 is the number of daughter nuclei present at time t_0,

D is the total number of daughter nuclei.

The total number of daughter nuclei present is given by:

$$D = D_0 + N(e^{\lambda t} - 1) \qquad (9)$$

This gives a basic equation which can be used to calculate the age of a rock if a realistic value can be assigned to D_0

and $^{238}U \rightarrow {}^{206}Pb$

can be viewed as if they were single decays.

The K-Ar system discussed in this work has a branched decay, in which ±11% of ^{40}K atoms decay by electron capture to an excited state of ^{40}Ar, which then emits a gamma ray with energy 1.46MeV, 0.16% of ^{40}K atoms decay by electron capture directly to the ground state of ^{40}Ar, and the remainder decay directly to the ground state of ^{40}Ca by β^- emission. (Faure, 1986)

The rate of decay of the parent nucleus is proportional to the number of nuclei remaining in the system.

Expressed mathematically:

$$\frac{dN}{N} = -\lambda t \qquad (1)$$

where λ is a constant of proportionality called the decay constant and n is the number of parent nuclei.
Integrating:

$$\int_0^t \frac{dN}{N} = -\int_0^t \lambda dt \qquad (2)$$

obtain:

$$\ln N - \ln N_0 = -\lambda t \qquad (3)$$

or:

$$N = N_0 e^{-\lambda t} \qquad (4)$$

CHAPTER TWO: ANALYTICAL TECHNIQUES

2.1 Geochronology and Isotope Geology

This chapter describes the first major portion of this work, being the application of geochronological techniques to the measurement of the rate and progress of geological processes over time, rather than merely determining the ages of individual samples or suites of samples. After a brief introduction to geochronology and isotope geology, the techniques which have been developed and applied to rocks from the Bushveld Magmatic Province are discussed in detail.

2.1.1 Basics of geochronology

All radioactive elements decay, with a specific decay constant (λ). This is related to the half-life of the element ($t_{½}$), the time taken for half of any given element to decay. Radioactive decay series are usually expressed as decays from parent to daughter, the daughter being a stable element at the end of the decay series. The decay can be either a single decay or a series of decays, with intermediate daughter products. An example of a single decay is found in the rubidium- strontium system.

$$^{87}Rb \rightarrow {}^{87}Sr$$

In this case an ^{87}Rb nucleus emits a β^- particle and becomes an ^{87}Sr nucleus.

The uranium-lead system comprises two decay series which are also branched. About 700 000a after closure, secular equilibrium is attained, where the rate of production of the Pb isotope at the end of the decay series equals the rate of decay of the U isotope. In all the U-Pb geochronology in this study, it is assumed that the system has reached this condition, and therefore the decay series:

$$^{235}U \rightarrow {}^{207}Pb$$

Zircon ($ZrSiO_4$) concentrates uranium on crystallisation, but excludes lead. Zircon is also highly resistant to weathering and therefore is an ideal mineral for use in dating techniques which rely on the U-Pb system.

Micas concentrate rubidium which substitutes for potassium, but contain virtually no strontium. This makes them highly suitable for Rb-Sr dating. They are however fairly susceptible to low temperature alteration, possibly making the assumption of a closed system invalid. For the mica ages, initial ratios were determined by analysing whole rocks and plagioclase. Plagioclase is ideal for the estimation of an initial $^{87}Sr/^{86}Sr$ ratio, as the mineral concentrates Ca (and Sr) and excludes K (and Rb) from its crystal lattice.

In all of the age determinations only the freshest material was used to try to minimise the possibility of isotopic systematics having been disturbed by alteration.

Table 1.1 Isotopic systems used in this study

Isotopic System	Parent	Daughter	Half Life
Rb-Sr	^{87}Rb	^{87}Sr	$4.88*10^{10}$ years
U-Pb & Pb-Pb	^{235}U	^{207}Pb	$.7038*10^{9}$years
	^{238}U	^{206}Pb	$4.468*10^{9}$years
K-Ar	^{40}K	^{40}Ar	$1.250*10^{9}$years

(Half lives calculated from decay constants quoted by Steiger and Jäger, 1977)

In this work, the emphasis has been placed on mineral ages, as these represent specific blocking temperatures as well as resulting in high precision ages. Minerals were selected which concentrate the parent element in any of these decay schemes and exclude the daughter element on crystallisation, but can hold the daughter element in their crystal lattice. This approach results in significant growth of the radiogenic daughter isotope over geological time periods, allowing precision dating without a large uncertainty in age resulting from the selection of an incorrect initial ratio. Variations in the initial concentration of the parent isotope will result in the development of considerable ranges of isotopic ratios of the daughter element, allowing the determination of high-precision ages.

As with any other radiometric dating, the following two assumptions must be satisfied if a radiometric age can be regarded as the true age of a rock or mineral suite:

1. The accumulation of the radiogenic daughter isotope has taken place in a closed system, i.e. a system where the isotopic and elemental systematics of the geochronometer have not been affected by any external influence.

2. All samples used in any determination have the same origin and the same initial isotopic ratios. In the case of the Bushveld Complex this condition is important, as samples may be collected from what appears to be the same rock unit at opposite ends of the complex, several hundred kilometres apart.

magma are identified in the stratigraphy by changes in this ratio. Contrary to the long intrusive period proposed by McCarthy and Cawthorn (*op. cit.*), it is believed that the changes in initial ratio are due to different sources for different magmas. This explanation is in line with the shorter cooling times discussed above.

It appears that the magmatic phase of the Bushveld Complex can be viewed as an "instantaneous" event, with respect to any of the currently available isotopic geochronometers. The timing of the processes between liquidus and solidus of the mafic rocks must therefore be addressed using other methods. Therefore in this work, the cooling from liquidus to solidus temperature is viewed as a single instantaneous event at 2054±1 Ma as indicated by the published data of Walraven and Hattingh (*op. cit.*). However, sub-solidus processes such as cooling, fluid movement and anomalous geothermal conditions may be studied using the available geochronological tools.

The rocks of the Bushveld Complex are often altered, often by a hydrothermal event penecontemporaneous with the intrusion (Cawthorn & Poulton, 1987, Balthaus & Stumpfl, 1985, Schiffries & Skinner, 1987). This causes a problem for geochronologists, as the alteration disturbs the isotopic systematics of the rocks. As a result of this alteration, many of the dates determined (see Walraven *et al.*, 1990) are younger than the age of intrusion.

1.4 Introduction to geochronology

This section is not an exhaustive look at geochr[illegible] but merely aims to introduce the techniques used in the study. The following isotopic systems were used in this study.

either a relatively short time span, slower plate movement than the present, or a continent-continent collision with little relative motion. (see Fig. 1.1) Field relationships indicate that the Lebowa Granite is younger than the mafic rocks of the Bushveld Complex, but the available geochronological studies indicate that these rocks are indistinguishable in age.

The palaeomagnetic data of Gough & van Niekerk (*op. cit.*) show that the tilting of the mafic rocks to their present orientation post-dates the imprinting of a direction of magnetisation onto the rocks. Later palaeomagnetic studies (Hattingh 1986a,b,c) confirm this conclusion. The coincidence of the magnetic poles for the Bushveld, Losberg and Phalaborwa Complexes, the Vredefort Granophyre, the Limpopo Gneiss and the extensions of the Great Dyke into the Limpopo Belt and the younger Waterberg sediments on the apparent polar wander path for Africa Layer *et al.* (1988) suggest that the intrusion of the Bushveld Complex was part of a far larger event, an event whose effects are seen throughout the Kaapvaal Craton. The coincidence with the *c.* 1.9 Ga Waterberg Group indicates elevated temperatures more that 100 Ma after the intrusion at 2054 Ma.

Currently, the thermal history of the Bushveld Complex and associated rocks is poorly constrained. Walraven (*op. cit.*) determined a time from intrusion to solidification of 350 000 years. A similar figure, 200 000 years, was determined by Irvine (*1970*). Both of these calculations used heat flow modelling. McCarthy & Cawthorn (1980) determined a cooling history of 40 Ma, based on the v .tion in initial $^{87}Sr/^{86}Sr$ ratio seen in the mafic rocks, assuming a number of intrusions from a single magma source, however most workers agree that this assumption is invalid. Another chronology for the cooling of the complex has been determined by Wright *et al.* (1983) using numerical modelling of trace element fractionation in magnetite, however this method also produced impossibly long cooling times, in excess of the age of the earth.

Kruger (1994) has studied the incremental development of the Bushveld Complex by compiling an $^{87}Sr/^{86}Sr$ initial ratio stratigraphy for the layered rocks. New influxes of

Lead chemistry is hampered by a further problem. Organic molecules readily adsorb heavy metals including lead. This provides a path for the ingress of lead into the laboratory, which cannot always be combatted using conventional means. It is believed that lead can be transferred to the distillate in distillations while adsorbed onto volatile organic molecules, and that ion-exchange techniques may allow the passage of lead into the final product in these cases, where it is not in an ionic solution. Organic molecules present a further problem in that they can suppress the ionisation of lead in the mass spectrometer. Techniques are therefore needed for the removal of organic compounds as well as the removal of dissolved ions from reagents.

H_2O

Water is purified using a Milli-Q water purification system, installed during the time of this study in the lab. This combines reverse osmosis and deionisation to produce water with a Pb concentration consistently below 10pg/ml. Distillation of this water in a Teflon two-bottle still consistently results in a lead concentration below 5pg/ml, with blanks of 1pg/ml having been recorded. This required no further improvement.

HCl

Hydrochloric acid was initially purified by several stages of sub- boiling distillation, vapour being evaporated off the surface of the liquid and condensed in a quartz glass still. The results that were produced using this technique were found to be highly erratic, often giving high lead blanks. During this work a number of experiments were conducted, and it was found that the best and most consistent results were obtained by at least one stage of boiling distillation.

An experiment was performed by Dr F.J. Kruger to investigate the performance of the boiling distillation technique in the purification of HCl:

3. "Purafil" filters, filled with granules of activated carbon, potassium permanganate and charged activated alumina. These adsorb and/or oxidise any material which comes through the bag filters.

4. Hepa filters are used as a final stage to remove any remaining material from the air and any dust shed by the Purafil medium.

The air is also cooled by an air conditioning unit and forced into the laboratory under pressure. This slight overpressure is needed to minimise the inward movement of airborne contamination through doors or other openings in the laboratory. Air is removed from the laboratory through fume hoods and passed through a scrubber which removes acidic fumes before the exhaust air is released into the atmosphere. The zircon lab receives its air upstream of all of the other laboratories, and is held at a slightly higher pressure which effectively seals it off from any source of contamination. Inside the laboratory, all critical procedures are performed inside plexiglass boxes, fed air by a fan blowing through a Hepa filter. This produces a pressurised, ultra purified micro-environment for chemistry and for the storage and drying of samples.

2.5.2 Purification of reagents

The largest sources of systematic and controllable contamination in the laboratory are the reagents used in the chemistry. Two methods may be employed to reduce sample contamination by reagents. The first and simplest is to reduce the reagent volumes used. The other and an equally important method is the purification of the reagents. These techniques are routine at the B.P.I., but further reduction of column and reagent blanks were necessary for this study, because of the low analyte concentrations and small sample sizes. For this reason, some of the standard purification techniques have been refined for use with small samples.

2.4.2 Hand-picking

The zircon samples were inspected under a binocular microscope, and contaminants such as chromite and baddeleyite were removed, using forceps or suction, applied through a syringe with the sharp point ground off the needle.

2.5 Chemical Procedures

A major part of this study was the analysis of small samples containing extremely low concentrations of the elements of interest. It was therefore necessary to critically examine existing procedures in the B.P.I. isotope laboratory and to modify these or, where necessary, develop new procedures for these analyses.

The successful analysis of small quantities of material requires high levels of precision in measurements and extremely low laboratory blanks. A special clean laboratory was used and developed, following the work of W Manton, discussed in detail in his report on the establishment of the facility at the B.P.I. (Manton, 1987), and clean chemical techniques were used throughout the process. In particular, the purity of laboratory air and reagents, the miniaturisation of the chemical techniques and good housekeeping practises ensured the low blanks recorded.

2.5.1 Purification of laboratory air

Air used in the zircon lab is purified through:

1. Coarse washable primary filters to catch microscopic dust.

2. Bag filters which remove much of the dust and other particulate matter in the air.

In the case of the granite samples both zircons were separated from the <250μm and 250-500μm fractions, while only the <250μm fraction was used in the case of the mafic pegmatoids.

2.4.1 Density and magnetic separation

The first stage in the zircon separation uses mineral density as a characteristic property of zircon. The first crude separation was performed on a Wiffley table. This was followed by the use of bromoform (g=2.83g/cc). The heavy fraction thus extracted consists of the heavy minerals, including zircon and some of the mafic minerals. The mafic minerals were removed using a Frantz magnetic separator. A current of 0.1-0.3A and a tilt of 5° proved sufficient to remove most of the mafics, especially in the case of the granitic samples, where hornblende is the major mafic mineral. Subsequent increases in current up to 0.5A removed most contaminants, leaving an almost pure zircon sample. This stage was followed by [illegible] liquid separation, using methylene iodide (g=3.31 g cm^{-3}). In this separation the sample was added to a test tube of methylene iodide, and agitated until all of the zircons had sunk. The lower half of the test tube was then submerged in liquid nitrogen, freezing the liquid inside and encapsulating the heavy minerals. The unfrozen upper portion of the liquid was then removed along with the lighter mineral grains, filtered and stored for reuse. The frozen portion was melted and washed into a filter paper lined funnel using acetone, and the heavy mineral fraction collected and washed with acetone. The waste methylene iodide/acetone mixture was poured into a beaker and allowed to evaporate, the vapour being removed by a fume extraction system. In certain samples large amounts of pyrite were separated along with the zircons. Pyrite is denser than methylene iodide and non-magnetic. This therefore had to be removed by dissolution in hot 2N HNO_3.

therefore be performed in a well ventilated environment with adequate fume extraction. It is recommended that alternatives, for example aqueous solutions of tungsten salts, be investigated.

2.2.1.3 Magnetic Separation

On the Frantz magnetic separator, crushed rock is allowed to run down a sloping aluminium ramp, which is slightly tilted at 5° to the horizontal, along its long axis. A magnetic field is applied, which pulls the magnetic minerals up this slope. At the end of the ramp, the minerals are dropped into two separate collectors.

2.3 Separation of micas from whole rock samples

Large mica crystals were separated from samples by physical removal with a hammer and small chisel, and then cleaned by scratching any small grains of the matrix mineral off the mica with the chisel point. Smaller mica flakes were separated from the matrix by preparing a light mineral concentrate on the Wiffley table and then the separation of the micas from this concentrate under a binocular microscope.

2.4 Zircon Sample Preparation

Several samples were selected for zircon analysis on the basis of observed abundance of zircons in thin section, or because of the high concentration of incompatible elements (eg. The mafic pegmatoids of the Layered Suite.) These samples were split into approximately 5cm blocks using an hydraulic splitter and these blocks crushed to about 1cm chips in a jaw crusher. The chips were then pulverised in a disc mill. The powder was separated into >500μm, 250-500μm and <250μm fractions. The >500μm fraction was returned to the milling stage.

The chemical separations are performed using ion exchange techniques specific to the elements of interest. These are described in detail in the following paragraphs.

2.2.1 Mineral Separation

All mineral separations rely on recognising definitive physical properties of the mineral of interest and using those properties to separate the mineral from the surrounding whole rock. The properties used in this study are visual appearance, density and magnetic susceptibility. Most minerals have a definitive appearance, and this can be used to separate them from a rock matrix, either by removing them from an intact rock, as was done for the large mica grains analysed, or by separating the mineral of interest from a rock crush under a binocular microscope. Minerals have a variety of densities and a number of methods may be employed to separate minerals of different density from one another.

2.2.1.1 The Wiffley Table

The Wiffley Table consists of a sloping metal surface, which vibrates while water is washed over it. Using a principle similar to that of the gold pan used by prospectors or the "Long Tom" used to separate gold from river gravels, the Wiffley table separates a rock powder into a number of density fractions, which are collected separately.

2.2.1.2 Heavy Liquids

Bromoform (density=2.83 g cm^{-3}) and methylene Iodide (density=3.31 g cm^{-3}) were also used for the separation of minerals on the basis of density. The crushed mineral is mixed with the liquid and the heavy fraction, which sinks, separated from the light fraction, which floats on the liquid. Care must be taken as these liquids are volatile, and the vapours are highly toxic. For this reason, the use of these liquids has been abandoned in most parts of the world (R. Arvidson, pers. comm.) All this work must

Table 2.2 Closure temperatures for isotopic systems in various minerals (data from Cliff (1985), Parrish (1990) and Keppie *et al.* (1993))

Isotopic System	Mineral	Closure Temp.	Reference
$^{40}Ar/^{39}Ar$	biotite	280±40°C	Harrison & McDougall (1980)
		300±50°C	Jäger *et al.*(1967), Purdy and Jäger (1976), Wagner *et al.* (1977)
		225-270°C	Turner & Forbes (1976)
Rb-Sr	biotite	464°C (phlogopite)	Giletti (1974)
		300±50°C (biotite)	Jäger *et al.*(1967), Purdy and Jäger (1976), Wagner *et al.* (1977)
U-Pb	zircon	650-750°C	Keppie *et al.* (1993)

Since the micas studied here are close to the phlogopite end member composition, a closure temperature approaching the higher estimate of 464°C is predicted (400±50°C has been used for the construction of Figure 6.1). For the $^{40}Ar/^{39}Ar$ data, the most encompassing estimate of temperature (300±50°C) will be assumed.

2.2 Laboratory Techniques

The laboratory techniques can be divided into three main sections: the separation of the mineral of interest from the whole rock, the chemical separation of the elements of interest from the sample and the isotopic analysis of these elements in the mass spectrometer.

interact with the walls of their container and will gradually evaporate, changing their concentrations. It is therefore important that spikes are constantly monitored.

2.1.6 Closure temperatures of isotopic systems

The principal aim of this work is not only to attempt to accurately date the intrusion of the Bushveld Complex, but also to attempt to determine its time-temperature history, using isotopic systems which "close" at different temperatures. Evidence discussed in the previous chapter suggests that the Bushveld Complex did not have a simple intrusive history, followed by rapid cooling and it should be possible to date not only the intrusive age, but also various points on the cooling curve which can be related to the closure of different isotopic systems. The following table summarises the closure temperatures of different isotopic systems in the minerals used in this study.

solution into two aliquots, one for the natural ratios and another for the concentration. This problem can be overcome by using a specially prepared ^{205}Pb spike. This problem does not arise for Sr analyses, as the $^{84}Sr/^{86}Sr$ and $^{84}Sr/^{88}Sr$ ratios are invariant and neither ^{84}Sr nor ^{88}Sr are involved in the age determination. A highly enriched ^{84}Sr spike is therefore used for Sr analyses, and the natural ratio is recovered from the spiked sample.

2.1.5.1 Sources of error in the Isotope Dilution method

An ideal spike contains only a single isotope, or in some cases a mixture of pure isotopes. In practice however this condition is difficult if not impossible to attain. There is therefore always a small concentration of the other isotopes of the element in question present. This can be measured and corrections made in the spiking process, but the uncertainty in the measurement of the spike ratio creates an immediate uncertainty in the concentration measured and the natural ratio recovered.

Mass spectrometric measurements are most accurate within a certain range, generally in the range 0.01 to 100. For smaller or larger ratios, the ion currents for the less abundant element become extremely low, the baseline measurement more critical and non-linearities in the measurement system more important. It is therefore important to calculate spike weights based on a reasonable estimate of the natural concentration and aiming at producing a spike ratio in this range. For small samples or at low concentrations it is often difficult not to overspike, unless a well calibrated weak (low concentration) spike is prepared. The mixed Rb+Sr spike for micas which was prepared as part of this study is an example of such a spike prepared specially for low concentrations of Sr and high concentrations of Rb. The mixed spike also has the advantage of eliminating weighing errors from the Rb/Sr ratio.

Care must also be taken in the preparation and storage of spikes, so that they do not become contaminated by the naturally occurring isotopes. This is of particular concern with expensive and scarce imported spikes. During storage, spikes will continually

2.1.5 Isotope Dilution

All the concentrations quoted for U, Pb, Rb and Sr were determined by isotope dilution (Moore *et al.*, 1973). In this method the sample is spiked with a known amount of solution of the element concerned of known highly enriched isotopic composition. From the isotopic ratios measured on the spiked sample it is then possible to accurately determine the concentration of the element. The spike used is usually very highly enriched (>99%) in one of the isotopes of the element of interest, eg. ^{84}Sr in the case of Sr and ^{235}U in the case of U.

Take for example the determination of rubidium concentration by isotope dilution.

$$^{87}Rb_{sample} = \frac{(\frac{^{85}Rb}{^{87}Rb})_{mix} - (\frac{^{85}Rb}{^{87}Rb})_{spike}}{(\frac{^{85}Rb}{^{87}Rb})_{natural} - (\frac{^{85}Rb}{^{87}Rb})_{mix}} \cdot \frac{AB}{C} \qquad (16)$$

where: A=^{87}Rb concentration in the spike

B=Mass of spike

C=Mass of sample

Since the natural $^{85}Rb/^{87}Rb$ ratio is constant (2.6), and this ratio is also known for the spike (0.0082), the ^{87}Rb concentration of the sample can be determined using the $^{87}Rb/^{86}Rb$ ratio measured with a mass spectrometer. From this the total Rb concentration can be determined.

This method is accurate for any concentration, provided that the final ratio for the mix is significantly different from either the natural material or the spike.

For U-Pb age determinations, the natural $^{207}Pb/^{204}Pb$ and $^{206}Pb/^{204}Pb$ ratios must be known for the age determinations. The only lead spikes at the B.P.I. suitable for the analysis of zircons are the ^{204}Pb and ^{208}Pb spikes. It is therefore necessary to split the

The degree of discordance is expressed as a percentage, and is calculated using the method described by Eglington & Harmer (1993). The percentage discordance is the ratio of the length of the line segment joining the plotted position of a sample and the concordia upper intercept, along that sample's discordia line, and the total length of the discordia curve, expressed in percent.

2.1.4.2 The $^{207}Pb^*/^{206}Pb^*$ method

The $^{207}Pb^*/^{206}Pb^*$ ratio can be used to calculate a model age for a rock. This method is used where uranium and/or lead concentrations are not available, for example in the zircon evaporation technique.

Combining the two equations used to describe the concordia diagram, we obtain:

$$\frac{^{207}Pb^*}{^{206}Pb^*} = \frac{^{235}U(e^{\lambda_{235}t}-1)}{^{238}U(e^{\lambda_{238}t}-1)} \qquad (14)$$

or:

$$\frac{^{207}Pb^*}{^{206}Pb^*} = \frac{1}{137.88}\frac{e^{\lambda_{235}t}-1}{e^{\lambda_{238}t}-1} \qquad (15)$$

since the present day $^{235}U/^{238}U$ ratio is 1/137.88.

The calculation of the radiogenic component of the $^{207}Pb/^{206}Pb$ ratio is reasonably simple, given that tables of values for average terrestrial leads exist for various ages. For minerals such as zircon, with very high initial U/Pb ratios, the contribution of common lead is extremely small, and in the evaporation method it is possible to "burn off" the common lead in the zircon before measuring the $^{207}Pb/^{206}Pb$ ratio such that a purely radiogenic lead ratio can be measured. The procedural details of this technique are discussed later in this chapter.

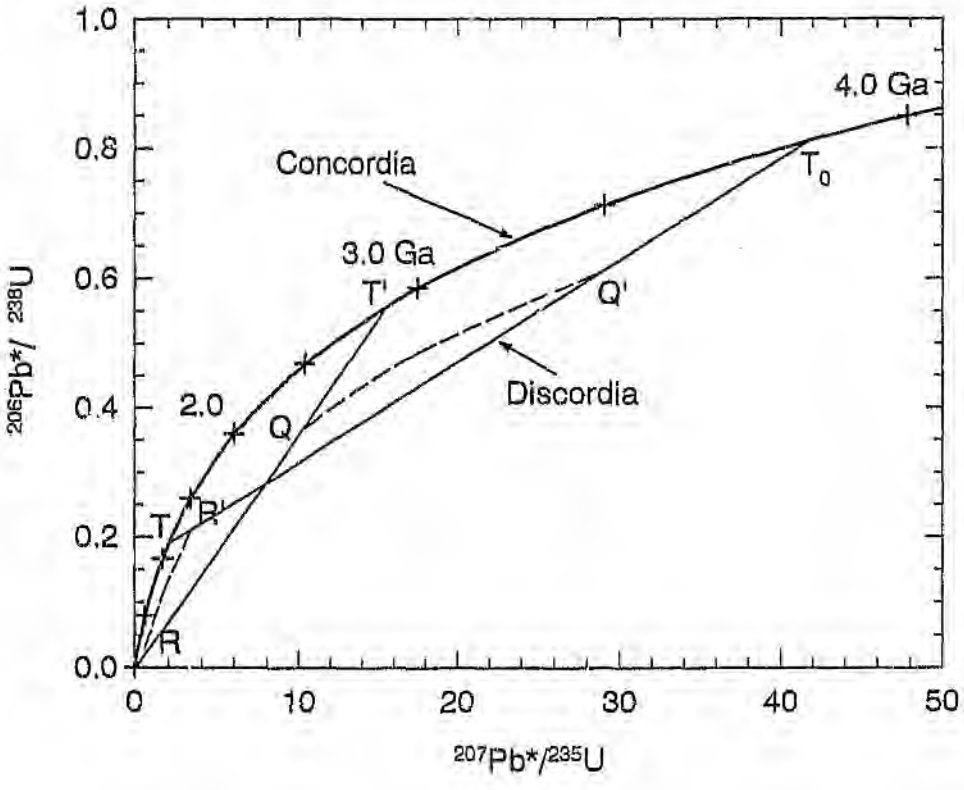

Figure 2.2 Concordia Diagram indicating the effect of episodic lead loss. [illegible] of samples of age T_0 lost lead at time T'. A sample which lost all it's lead would plot at the origin and the Pb/U ratios would grow along concordia to point T, indicating the age of the lead loss event. Samples which lost only a portion of their lead, for example samples Q and R, grow along new growth curves such as Q-Q' and R-R', and define the discordia chord $T\text{-}T_0$, with upper and lower concordia intercepts giving the true age of the suite of samples (T_0) and the age of alteration (T). Note that $T_0\text{-}T=T'$.

3. After a week or two, the bomb is removed from the oven, allowed to cool and the PTFE beakers are removed. The solution in each is decanted into a cleaned Savillex beaker and checked for complete dissolution. If all the sample is not dissolved, the sample is returned to the PTFE beaker and put back into the oven.

4. The solution is dried down and the sample dissolved in a 1ml of clean 6N HCl. This solution is split 3:1 between an unspiked PTFE beaker and one which has been spiked with 99% ^{204}Pb spike and 99.9% ^{235}U spike solutions. The spike beakers and natural beakers are kept separate through all procedures such as cleaning, and any beaker which has ever contained the ^{204}Pb spike can not be used for unspiked samples as the ^{204}Pb can easily contaminate samples.

5. The lead is separated from the natural sample and the lead and uranium from the spiked sample using a Teflon micro-ion exchange column containing a small amount of anion exchange resin.

6. The resulting solutions were dried under a heating lamp in a clean air box.

The total method blank for lead using this technique has been measured at 150pg.

2.7.3 Mass Spectrometry

Zircon samples contain at most a few 10s of nanograms of lead, and a special philosophy is needed for their analysis in the mass spectrometer. The technique used during this study involved two stages. Data were initially collected using extremely small beam currents (of the order of 10^{-13}A), and the single Daly collector on the VG354. Following several blocks collected using this technique, the program specified a static multi-collector routine, using the five Faraday collectors. This technique

automatically aborted the analysis. The ion beam was measured using a three collector measurement routine, with beam currents of up to $1.5*10^{-11}$A.

2.7 The Conventional zircon technique

2.7.1 Laboratory Procedures

In the conventional zircon technique, zircon samples are dissolved and the lead and uranium separated using ion exchange techniques. The concentrations of Pb and U in the sample are determined by isotope dilution. Zircon separates were prepared from two of the mafic samples, LF1 and WV1. These were then examined under a binocular microscope, and a few milligrams of fresh inclusion-free zircons selected. In both samples only one zircon fraction was identified and none of the zircons appeared to include overgrowth phases. During the chemical separation it is vital that laboratory blanks are kept to an absolute minimum, as the small size of the samples and extremely radiogenic $^{206}Pb/^{204}Pb$ ratios mean that any contamination will ruin a sample. The methods described in section 2.5 were employed to minimise the laboratory lead blank.

2.7.2 Chemical Separation of Lead and Uranium

The separation of Pb and U from zircons is performed using extremely small reagent volumes in Teflon micro-columns.

The following procedure is followed:

1. A few mg of clean zircons are weighed into small PTFE beakers.

2. The beakers are covered with loose fitting lids and placed together with ~5ml of distilled 48% HF into a Teflon bomb. The bomb is placed inside a steel jacket and heated in the oven to 200°C.

tantalum filament and dried down at a filament current of 1.2A. This bead was loaded into the mass spectrometer and outgassed at the following filament currents:

Side : 0.5A
Centre: 1.6A.

Initial currents of 0.6 A on the side filament and 1.8A on the centre filament were used for the analysis, and these and the focus settings were adjusted to give an optimum ion beam.

Data were collected in blocks of 8 ratios, and sufficient data were collected to give a standard error <0.1% and a standard deviation <0.5% of the ratio measured.

Strontium

Sr analyses were performed on the VG 354 Mass spectrometer, running in fully automatic mode. After drying the sample down in nitrate form, it was loaded onto a single Ta filament as follows:

1. A small current was applied to slightly heat the filament, allowing two lines of Parafilm to be melted onto it, approximately 1mm apart.

2. The sample was picked up in 2 μl of H_3PO_4, and loaded onto the filament.

3. The drop of liquid was evaporated at a filament current of 1.3A after which the filament current was gradually raised until the filament gave off a dull red glow. In this process, the lines of parafilm were burnt off the filament.

An initial filament current of 1.6A was used for the analysis, and this current and the focus settings were adjusted automatically to give an optimum ion beam. A maximum current of 3.0A was specified and if this current was reached, the machine

beam is generated, in the cases discussed here by the direct heating of the sample. The beam is accelerated through o potential difference of 8kV and fired into a magnetic field aligned normal to the direction of the ion beam. The beam of ions follows a circular path through the instrument's flight tube in the magnetic field, with a radius proportional to the mass of the ion (dependent on the isotope) and the kinetic energy (constant at 8keV). The beam strength is measured by a collector or array of collectors at the end of the flight tube of the instrument.

The deflection of the beam is dependent on the energy of the incoming ions and the mass of the ions. It is therefore possible to separate ions of different masses into separate beams and to measure the ratios of the intensities of these ion beams. This can be used to measure the isotope ratios of a specific element in a sample.

Three mass spectrometers were used during this study, the VG Micromass 30 and VG354 instruments at the B.P.I. and the Finnegan MAT261 at the Geological Survey of South Africa laboratory in Pretoria.

The VG354 and the MAT261 are both fully automated, whereas the Micromass 30 (MM30) is a manual instrument, with a computer controlled data acquisition system. The MM30 has a Faraday collector for the collection of data and a Daly Electron Multiplier for use during aiming and focusing. On the two automated instruments, the electron multiplier can also be used for the collection of data. These instruments are also equipped with multiple Faraday collectors, allowing the simultaneous measurement of five ion beams on the VG354 and seven in the case of the MAT261. The zircon evaporation analyses were performed using only the Daly Collectors.

Rubidium

Rb analyses were performed on the VG Micromass 30 mass spectrometer. The dissolved, spiked sample was loaded onto the side filament of an outgassed double

3. The sample was dissolved in 5-10ml of distilled 48% HF and a few drops of distilled nitric acid. The solution was then dried down.

4. The resulting fluorides were converted to chloride by filling the beaker with distilled 6N HCl to dissolve the solid matter and drying the resulting solution down.

5. These solids were then dissolved in 1.5ml of distilled 2.59N HCl, and any remaining solid matter separated in a centrifuge. The centrifuge tube was kept, as the few drops of solution remaining inside the tube were used for the rubidium runs.

6. Rb and Sr were separated from the solution by ion exchange, using cation exchange resin and dried down.

7. Sr samples were dissolved in a small amount of HNO_3, and dried down again to convert to nitrate and reduce organic contamination.

Laboratory blanks were kept to a minimum by using only distilled reagents and adhering to the laboratory procedures discussed in the previous chapter. The Rb and Sr chemistry was performed in a different laboratory to the U and Pb analyses, also supplied with pressurised filtered air.

Total method blanks were measured at: Rb - 100pg
Sr - <1ng

2.6.2 Mass Spectrometry

All isotope dilution and isotopic ratio data reported in this study were determined using a mass spectrometer. This instrument measures the ratios between isotopes of different mass. The operation of the mass spectrometer is relatively simple. An ion

For example care must be taken that reagents are never left open or poured in such a way that the contents of a stor' 'ssel are ever at risk of contamination. It is inadvisable to reach over any open vessel, and care must be taken in the opening and closing of beakers and bottles. Handling of laboratory equipment should be kept to an absolute minimum and all procedures should be carefully thought out to involve the minimum of handling. Ideally all procedures should be carried out in clean air boxes which are kept closed for as long as possible.

The effects of these cleaning procedures and laboratory practices are seen in the different blanks measured by different analysts using different beakers. An inexperienced worker, using beakers usually used in the conventional lead laboratory measured total method blank levels twenty times those quoted in this study.

2.6 The Rb-Sr Method

2.6.1 Chemical separation of Rb and Sr

The following method was used for the separation of Rb and from the mica.

1. The dissolution beaker was spiked with a specially pr 'ed Rb+Sr spike in the case of micas and separate Rb and Sr spikes for the ga. '. plagioclase and whole rock samples. The exact ount of spike used was weighed to 5 decimal places, with a correction for evaporation made by weighing the spike over a measured period of time and extrapolating the resulting curve back to the time of spiking. The amount of spike was calculated to produce an optimum isotopic ratio for a rough estimate of the concentration of the element in the sample.

2. Approximately 0.1g of sample was weighed into the beaker.

A set of bomb capsules was then made by B.P.I. technician, Johan Holtzhausen, using a Teflon rod, produced from Teflon powder which had been leached in hot aqua regia for several weeks. At the time of completion of the practical portion of the project, these capsules still had a higher lead blank than the older ones, but this was still decreasing and is being monitored.

2.5.4 Good Housekeeping

A potentially important source of contamination in the laboratory is the analyst. This contamination may be random and episodic, and is not easily detectable. S/he walks from the dirty outside environment into the clean laboratory, and can carry all sorts of contaminants on his/her skin, clothing and hair. It is therefore necessary that as much of the analyst, especially skin and hair be covered.

Lead levels in Johannesburg air are extremely high (pers comm. W. I. Manton). In addition to posing a threat to health, this lead is adsorbed onto particulate matter in the air, which may become attached to the analyst's person. It is therefore essential that any exposed areas of skin are thoroughly washed before entering the lab, and that cyclists or motorcyclists shower and change their clothing before entering the lab. The atmospheric uranium levels are also extremely high due to the uranium in the dust from mine dumps. This can also contaminate the analyst, and similar precautions must be taken as for lead.

These two factors, the atmospheric and the personal, are probably the limiting factors for the lead and uranium blanks in the B.P.I. isotope laboratory. It should however be possible to reduce the effect of the atmospheric blank still further until it becomes negligible. The personal blank is specific to every analyst, and can be reduced if clean laboratory procedures are carefully thought out and practised until they become second nature.

Table 2.4 Reagent and total method blanks achieved

Reagent	Pb Blank
H_2O	<5pg/ml, as low as 1pg/ml
HCl	2-3pg/ml
HNO_3	10pg/ml
HF	<10pg/ml
8.8N HBr	7.5pg/ml
0.6N HBr	2pg/ml
H_3PO_4 - silica gel mix	3pg/2.5μl load
Dissolution in Teflon bomb	30pg
Total method blank	150pg

2.5.3 Control of blanks due to the dissolution bomb and other labware

While Teflon labware is generally clean, small amounts of impurities do exist in the raw materials used. Generally these are of little concern, as their contribution to the blank is orders of magnitude less than other sources such as reagents. In this study, small low-level samples have been analysed and the labware blank begins to make a significant contribution to the total lead content of a sample. The dissolution bomb is a major source of contamination of zircon samples as much lead can be leached from the Teflon in the week or two taken for each dissolution in HF at high temperature and pressure.

Repeated leaching of Teflon beakers in strong acids has been found to gradually remove all the mobile lead, and for this reason clean labware is stored in HCl and then well rinsed before use. The small Teflon capsules used for dissolution were also repeatedly cleaned in the bomb under high temperature and pressure in HCl and HF in an attempt to remove all mobile lead. Over time this approach reduced the dissolution blank from up to 1ng to around 30pg.

Table 2.4 Reagent and total method blanks achieved

Reagent	Pb Blank
H_2O	<5pg/ml, as low as 1pg/ml
HCl	2-3pg/ml
HNO_3	10pg/ml
HF	<10pg/ml
8.8N HBr	7.5pg/ml
0.6N HBr	2pg/ml
H_3PO_4 - silica gel mix	3pg/2.5μl load
Dissolution in Teflon bomb	30pg
Total method blank	150pg

2.5.3 Control of blanks due to the dissolution bomb and other labware

While Teflon labware is generally clean, small amounts of impurities do exist in the raw materials used. Generally these are of little concern, as their contribution to the blank is orders of magnitude less than other sources such as reagents. In this study, small low-level samples have been analysed and the labware blank begins to make a significant contribution to the total lead content of a sample. The dissolution bomb is a major source of contamination of zircon samples as much lead can be leached from the Teflon in the week or two taken for each dissolution in HF at high temperature and pressure.

Repeated leaching of Teflon beakers in strong acids has been found to gradually remove all the mobile lead, and for this reason clean labware is stored in HCl and then well rinsed before use. The small Teflon capsules used for dissolution were also repeatedly cleaned in the bomb under high temperature and pressure in HCl and HF in an attempt to remove all mobile lead. Over time this approach reduced the dissolution blank from up to 1ng to around 30pg.

Hbr

Clean 0.6N HBr is produced by distilling 8.8N HBr in quartz sub- boiling still, to produce 8.8N HBr with a lead concentration of 7.5pg/ml. This is then diluted to 0.6N HBr using the cleanest water available. The resulting reagent blank is therefore controlled by the blank of the water, the HBr contributing less than 1pg of lead to every millilitre of reagent.

Loading reagents

The loading reagents, silica gel and phosphoric acid are prepared separately and then mixed. Si-gel is produced by reacting $SiCl_4$ with 0.6N HBr, to produce a Si-gel-HBr mixture. This mixture is then passed repeatedly through an anion exchange column to remove lead.

0.1N H_3PO_4 is produced by reacting P_2O_5 with 0.6N HBr and passing the resulting P_2O_5-HBr mixture through the same column as the Si-gel. In both processes the HBr acts only as a carrier, the distribution coefficient for Pb on the resin used being highest in that normality of the acid (Manton, *op. cit.*).

The H_3PO_4 - silica gel mix produced from these two reagents gives a total loading blank of 3pg per 2.5μl load. This is still somewhat high, but is adequate for the samples studied here.

The blanks thus obtained are summarised in Table 2.3, below.

HNO_3

Nitric acid was also initially produced in a quartz sub-boiling "fishbowl" type still and then later produced in a two bottle sub-boiling still. The distillate from either of these techniques was then further purified by sub-boiling distillation in a Teflon two bottle still, using the technique of Mattinson (1972).

HF

Hydrofluoric acid cannot be distilled in glass stills, as the acid dissolves silicate materials. This reagent is therefore double distilled in a Teflon FEP two bottle still. In these distillations only the middle third fraction of the distillate is collected, as this fraction has been found to contain less Pb than the first and third fractions. Again it is believed that organic molecules play a major role in the transport of lead in the distillate (pers. comm. W.I. Manton). These organics will however be volatilised early in the distillation process, carrying lead to the first distillate fraction. The higher lead concentration in the last fraction results from the transfer of ionic lead from a solution which has been enriched in ions by the removal of the first two fractions of distillate.

The actual blank of the acid is not the only factor governing the total Pb contamination in an analysis. Rather more important for zircon work is the dissolution blank measured in the dissolution bomb. The HF is transferred to the sample in the vapour phase, which is in effect a further distillation process. Of course, as with all distillations, the quality of the initial product is critical in ensuring a clean distillate. The other contributor to the dissolution blanks is the lead leached from the Teflon of the bomb, so while the HF has a lead concentration of <10pg/ml, the dissolution blanks are of the order of 30pg from considerably less than 1ml of reagent used. This indicates that the Teflon bombs are the major source of contamination in the dissolutions. This blank will diminish with continued use of the bombs, as the repeated exposures to highly acidic atmosphere leach lead from the Teflon bomb capsules.

4l of approximately 6N HCL (produced by mixing 2l of stock ANALAR with 2l of Milli-Q purified water) were distilled in a boiling still, and the Pb content of a number of fractions determined. The following results were obtained:

Table 2.3 Pb content of various distillate fractions from a boiling distillation of 6N HCl

Fraction	Pb Concentration
First 5ml	67pg/ml
Sample at 250ml	13pg/ml
Sample at 1000ml	11pg/ml
Sample at 2000ml	8.3pg/ml
Sample at 3000ml	12pg/ml
Residue in still pot	13μg/ml

These results show that there is initially a transfer of Pb in the vapour phase, after which a consistent, high-purity product is produced. The distribution coefficient at boiling between liquid and vapour is *c.* 10^6.

Sub-boiling distillation of small amounts of this acid in a quartz still then produced acid with a lead blank of 2-3pg/ml. It is suggested that the boiling process may break up organic molecules which are lost to the process by evaporation and carried through the boiling still in the first fraction of distillate, and that these organic molecules carry away a significant fraction of the lead in the stock solution of acid.

A boiling still is thus apparently desirable to produce an "organic free" product with a reproducible blank. A second boiling distillation was not attempted as a quartz glass boiling still was not available, but would have been necessary to produce a cleaner product that could be produced in a conventional borosilicate glass still.

The results are shown graphically (see Fig. 3.1). Regression of these data using the method of York (1969) yields an errorchron (MSWD=8.04) age of 2025±12 Ma. This age is within error of Walraven's (1991) age of 2061±27Ma, but is slightly younger than Armstrong's unpublished age of 2054±1, and Walraven and Hattingh's (1993) age for the younger Nebo Granite of 2054±1.8Ma. This suggests mild alteration, which is indicated by the greenish colour seen in the WV and LF micas in thin section. The other mica samples are however apparently fresh. The simple explanation of a slight lowering of the age by chloritisation does not explain the inter- and even intra-granular variability in the ages of these micas.

The age determination is therefore believed to represent more than simply the slight lowering of age associated with alteration. It is suggested that the cooling from the solidus to the blocking temperature for the Rb-Sr system (approx. 600°C) may have occurred over an extended period. Below this temperature, continued elevated temperatures may have allowed the intra-granular movement of Rb and especially radiogenic ^{87}Sr. The Sr^{++} is considerably smaller than the ^{+}Rb ion, and has an additional charge. It will therefore be relatively mobile in the K site of a phlogopite crystal lattice, and could move around inside a large mica grain, or be removed from the grain during an alteration event, causing large variations in apparent Rb-Sr model ages, where these are determined on small parts of individual grains.

The analytical data from two of the samples (WV2 mica 3 and WV2 m1 rim1) plot far from the regression line through the data, and these were therefore excluded from the final regression.

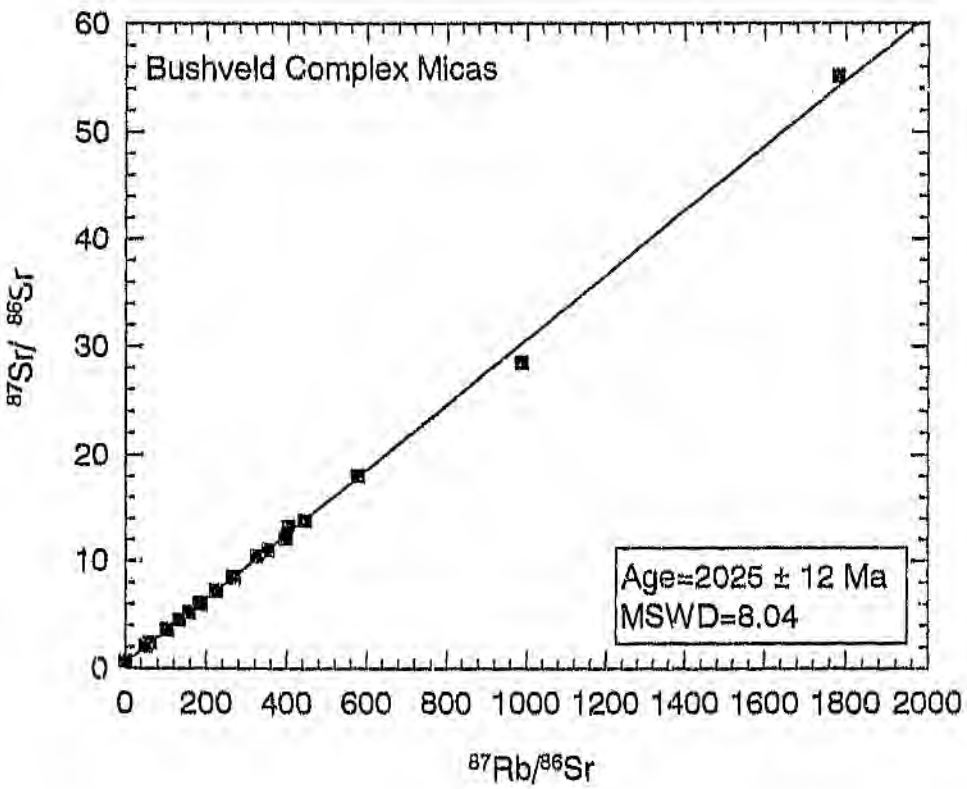

Figure 3.1 Isochron diagram, showing the results of analyses of Bushveld Complex mica, plagioclase and whole rock samples.

Table 3.1 Results of the Isotopic Rb-Sr isotopic analyses of mica, plagioclase and whole rock samples from the Bushveld Complex (Model Ages calculated using an Initial $^{87}Sr/^{86}Sr$ ratio of 0.7058, calculated from the micas, plagioclase and whole rock samples)

Sample	Rb	Sr	$^{87}Rb/^{86}Sr$	$^{87}Sr/^{86}Sr$	Model Age
WV2m1 rim1	396.20	4.069	1782.131	55.150	2119
WV2m1 rim2	390.00	5.353	576.6942	18.014	2082
WV2m1 int	390.00	6.019	396 4523	12.103	1996
WV2m1 core	390.80	9.463	181.5867	6.0206	2032
WV2m2-1	371.20	7.130	264.7149	8.4500	2031
WV2m2-2	180.80	2.990	351.1020	11.000	2035
WV2 mica3	376 80	4.104	986.3614	28.442	1953
WV3 mica	374.40	11.300	131.9763	4.5588	2027
LF4 mica	578.38	15.478	156.1590	5.2502	2020
NG2 754.00	383.00	8.118	223.7882	7.2443	2028
NG2 773.65	484.30	17.700	101.7414	3.6230	1991
P2 Biotite	646.50	9.607	443.4388	13.767	2044
RGC-1	370.60	8.733	187.0272	6.05657	1986
P-2r	607.00	9.675	402.9261	13.17591	2146
P-2	608.20	10.63	323.3946	10.45534	2091
FF1 100	340.50	19.30	59.6996	2.44109	2018
FF1 101	361.60	24.10	49.4385	2.12706	1996
WV3 wr	4.28	36.130	0.3430	0.71576	
WV2 plag	1.12	87.374	0.0371	0.70727	

LF4

LF4 is an extremely coarse grained feldspathic pegmatoidal pyroxenite, collected in the Lefkochrysos (now Crocodile River) platinum mine.

P2 Biotite and the two NG2 samples are mica separates, collected by F J Kruger and researchers from the Geology Department of Rhodes University respectively. Samples **P2 and P2r** are reanalysed samples of a cleaner mica separate from sample P2. Sample **RGC-1** is a mica separate supplied by Dr R G Cawthorn of the Department of Geology, University of the Witwatersrand, while samples **FF1-100** and **FF1-101** come from the Fairfield Borehole, and were supplied by Dr F Walraven of the Council for Geoscience.

All these micas appear fresh in handspecimen, however petrographic investigations of all of these samples indicate a degree of chloritisation. This is seen in the greenish colour of the phlogopites in thin section.

3.4 Results

The samples described above were analysed using the techniques described in Chapter Two. All the mica analyses were performed using the mixed Rb+Sr (mica) spike. This spike was calibrated against weighed standards and standard feldspar SRM-607.

The results obtained are presented in Table 3.1

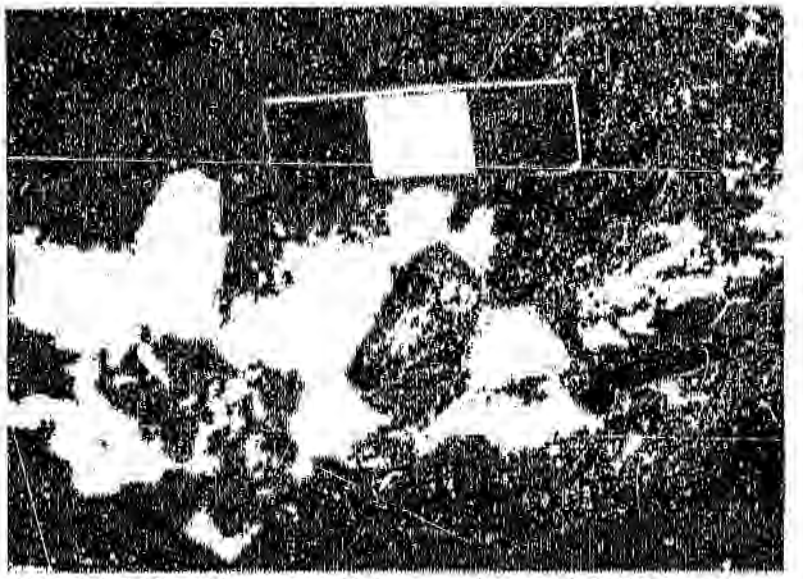

Plate 3.1 Feldspathic pegmatoidal pyroxenite sample WV2 (Note large mica grains)

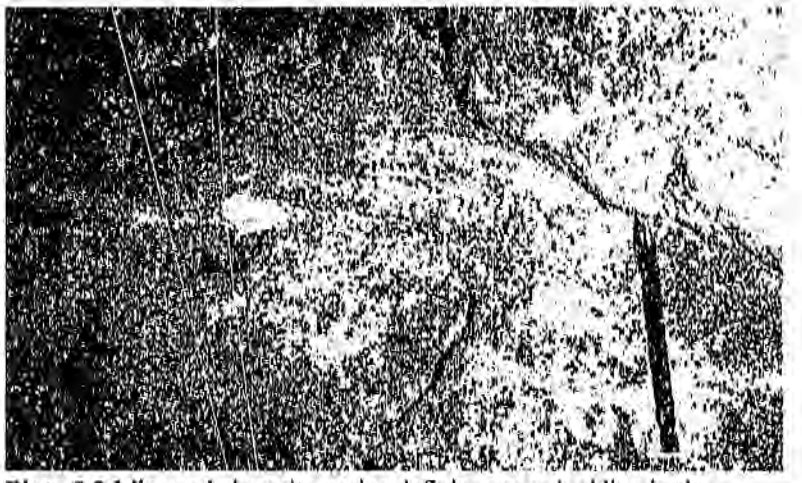

Plate 3.2 Mica and chromite grains defining cross-bedding in the locality of dunite sample WV3.

of mica. They are not to be confused with the mafic pegmatites found in the area, which crosscut the stratigraphy, eg. the Driekop Pipe.

A large mica grain was separated from the rock sample (See Plate 3.1). A flake from the centre of the grain was then cut into three approximately concentric rings, with the c-crystallographic axis at their centre. This sample is referred to as WV2 mica 1. Within this grain was a lath of plagioclase, oriented parallel to one of the crystal faces. This grain, and others were also analysed (as WV2 plag) to determine an initial $^{87}Sr/^{86}Sr$ ratio.

Two samples, referred to as WV2 mica 2, were separated from another large mica grain. These were cut perpendicular to the c-axis.

A number of randomly sampled flakes of mica from a third grain were analysed together to provide an average mica sample. This has been called WV2 mica 3.

WV2 plag

A plagioclase sample was also separated from this rock, to provide an initial $^{87}Sr/^{86}Sr$ ratio.

WV3

WV3 is a dunite sample from the same mine. In this sample, flakes of mica and small grains of chromite define cross-beds on exposed surfaces observed during a visit to Winterveld chrome mine (Plate 3.2). This is indicative of the movement of the partially crystallised rock in the magma chamber in a fashion not unlike the movement of sediment. A conventionally separated mica separate of flakes from a coarse crush was used in the analysis of this sample. A whole rock crush from WV3 was also analysed.

3.3 Sampling, petrography and sample preparation.

Micas are common in igneous and metamorphic rocks, and their cleavage and distinctive appearance makes their separation from a whole rock crush easy by physical means and hand-picking.

The sampling program aimed to collect samples with minimal alteration and mica grains large enough to allow single grains or portions of grains to be analysed. These large mica grains abound in the pegmatoidal rocks of the Critical Zone (such as the Merensky Reef and pegmatoids associated with the chromitite layers), and fresh samples can be collected at a number of underground localities.

Mica separates were produced in two ways. Where single large mica grains were to be analysed, these were removed from the surrounding rock using a small chisel, care being taken not to damage the mica grain. Any grains of host rock that adhered to the micas after this was scratched off with the chisel. The large mica grains were divided into sections with a scalpel where cuts ran parallel to cleavage and with scissors where the cuts were made along perpendicular to the cleavage.

In samples where many small mica flakes were needed, for example the dunite, WV3, the samples were crushed to +500 microns, and the light and heavy minerals separated using a Wiffley table. The mica was then removed from the lighter fraction and was then hand picked under a binocular microscope.

3.3.1 Sample Descriptions

WV2

Sample WV2 is a coarse feldspathic pegmatoidal pyroxenite. Pegmatoid and pegmatoidal refer to rocks with a pegmatitic texture that occur conformably with the country rocks. These rocks formed at the same time as the finer grained rocks that coexist with them and have been chosen for this study as they contain large quantities

CHAPTER THREE: Rb-Sr ANALYSIS OF MICAS FROM THE MAFIC PHASE OF THE BUSHVELD COMPLEX

3.1 The mica Rb-Sr geochronometer

Micas are often used for Rb-Sr geochronology for several reasons. Most important, they have initially high Rb concentrations, Rb substituting for K in the mica lattice, and very low Sr concentrations. Consequently, with time highly radiogenic $^{87}Sr/^{86}Sr$ ratios evolve, allowing ages to be determined to a high degree of precision.

However, Fe-Mg micas are relatively susceptible to alteration in a variety of geological environments. This can result in open system behaviour and partial or total resetting or disturbance of the isotopic systems. As will be seen in this work, the alteration of micas is not always easily apparent on initial inspection.

3.2 Aims of the mica Rb-Sr study

The primary aim of the Rb-Sr mica study was to attempt to determine the absolute age of the Bushveld Complex, using the model age technique. Given the possible protracted cooling period of the complex, the mica technique was chosen as it is blocked at a temperature below the solidus temperature of the rocks. Different zones of an extremely large mica grain were analysed separately to see if there were different ages recorded by different zones within the grain and if the Rb/Sr ratio varied during crystallisation.

A general examination of the Rb-Sr system in the rocks was also undertaken to determine the specific systematics and the suitability of Rb-Sr mica model ages for high precision geochronology.

cases no data were collected using the double filament technique, and the data collected during the evaporation process have been used.

2.9 Summary and Conclusion

The analytical techniques employed for this study are the Rb-Sr technique, on micas and garnets and the U-Pb and $^{206}Pb/^{207}Pb$ techniques on zircons. In all isotopic analyses, especially U-Pb work on zircons, which have low Pb concentrations and are uncommon in most rocks, giving resultant small sample volumes, it is necessary to minimise the analytical uncertainties. This necessitates the minimisation of laboratory blanks, and a large portion of the analytical work in this study was devoted to the minimisation of laboratory blanks, especially Pb blanks.

The techniques described in this chapter have been used successfully to attain the blank levels needed for the analysis of small low concentration samples, although the total method lead blanks are still too high for successful single grain analysis. This will presumably improve with time, as labware becomes cleaner, and as analysts become more experienced. The proposed introduction of lead free petrol in 1995 should also improve the atmospheric lead blank, and allow lower Pb blank levels to be achieved.

The improvement in the blank levels, and low level analytical techniques in the B.P.I. laboratory should facilitate future development of low level Pb analyses of zircons, and other small samples.

emitted is aimed at the evaporation filament. The loading procedure is easier if it is performed under a binocular microscope.

2.8.2 Mass Spectrometry

Double filament

The loaded bead is mounted in a turret, which has been modified to be able to run double filaments. (The normal configuration allows only single or triple filaments to be used.) The side filament is heated up to a yellow glow, the ^{206}Pb peak is located by scanning in the approximate mass range for the 206 peak and the beam strength is maximised manually, using the focus unit. It is important that the filament current is not set too high at this stage, as only the most easily evaporated lead must be analysed. At this stage data are collected manually, moving between the ^{206}Pb and ^{207}Pb peaks. When the beam's intensity is close to zero, i.e. when the first fraction of zircon has been completely evaporated, the side filament current is turned down to zero, and the centre filament is heated up. The evaporated lead is now analysed manually. At the end of this analysis, the filament current is increased to burn off any remaining traces of condensate, and the process repeated with a slightly higher side filament current. This allows the analysis of several zones of a multi-zone zircon. All isotope ratio measurements are made manually, as the automated routines respond to low beam strengths and decreasing beam strengths by increasing the filament current. For such small samples this could have disastrous consequences. On the Finnegan machine, the process is similar, but is simplified by the presence of an optical pyrometer. This allows a quantitative control over the side filament temperature.

Single Filament

This technique is far simpler, but often gives less stable ion beams than the technique described above. Here, data is collected directly from the evaporating zircon, and beam stability is a function of the randomness of the evaporation process. In some

predict, using a simple model of alteration, with the outer, most fractured and most radiation damaged portions of the zircon evaporating first and leaving a less altered fraction for the later analyses. In practise the concordance or discordance is monitored by observing the non-radiogenic lead isotope ^{204}Pb.

In this study two mass spectrometers were used for the zircon evaporation technique, these being the Finnegan MAT 261 instrument at the South African Geological Survey laboratory in Pretoria and the VG354 at the Bernard Price Institute of Geophysical Research at the University of the Witwatersrand, Johannesburg. The techniques used are essentially similar, the differences in loading techniques for the different filament designs and the use of a pyrometer on the MAT 261. The method used on the VG354 is described in detail and the method used in the Geological Survey Laboratory has been described by Walraven & Hattingh (1993)

2.8.1 Filament Preparation and loading

The VG354 is designed to use triple filaments, in which the two outer filaments are connected in series and the centre filament operates on a separate circuit. On the conventional triple filament, the two side filaments are positioned parallel to each other, with the centre filament perpendicular to these.

The evaporation technique demands a double filament arrangement, with the two filaments facing each other, but connected to independent circuits. A normal triple bead is modified so that the centre filament legs are connected to one side filament and the centre filament posts are removed. The bead is strung with rhenium ribbon 1mm wide (twice the width used for conventional mass spectrometry.) The evaporation filament is bent parallel to its length, to make a boat shaped space, inside which a zircon can be loaded. The bead is cleaned and outgassed for 10 minutes at 5A. The emission filament posts are bent back to allow easy access to the evaporation filament, and the zircon to be analysed is placed in the "boat" in the rhenium filament. The boat is then crimped closed and the slit through which the vapour of the zircon will be

allows the analysis of extremely small samples using the Daly collector before the filament current is turned up to the temperature needed for the Faraday collectors. The higher filament temperatures needed for the Faraday collectors may burn the sample off the filament before data can be collected.

2.8 The Zircon Evaporation Technique

In conventional "wet chemical" methods, lead is separated from zircons and a lead solution is loaded onto a mass spectrometer filament using silica gel. In this process, the silica gel bed acts as an emitter, increasing the degree of ionisation of the lead, producing good results in the instrument.

The idea of using zircon material as the emitter is not new. Zykov & Stupnikova (1957) described the analysis of lead isotopes in zircon using a single filament, with the zircon embedded in that filament. Kober (1986, 1987) further developed this technique, using a double filament arrangement, with a zircon embedded in one filament, which serves as the evaporation filament. Lead evaporated from the zircon is deposited, together with other components of the zircon on the ionisation filament. Lead isotope ratios are then determined using this filament. In this technique HfO_2 and SiO_2 act as an emitter.

The advantage of this technique over the conventional wet chemical technique are obvious. There is no pretreatment of the zircons, making the technique fast and simple. In addition, lead blanks are minimised, as no treatment or loading reagents are used, and there is no treatment of the zircons in the laboratory.

The evaporation technique cannot however provide any information about the concordance or disconcordance of the zircons or uranium concentrations. Only the $^{207}Pb/^{206}Pb$ age can be determined. It is therefore assumed that the zircons used for such an age determination are concordant. It is however possible to burn discordant fractions off the zircon early in the age determination, if these behave as one would

CHAPTER FOUR: URANIUM-LEAD AND LEAD-LEAD ANALYSIS OF ZIRCONS FROM THE BUSHVELD COMPLEX

4.1 Introduction

Zircon is an ideal mineral for high precision U-Pb geochronology, as it concentrates uranium, excludes lead, and is extremely resistant to alteration. Unfortunately, zircon is not generally abundant in mafic rocks such as those of the Bushveld Complex, as these rocks do not generally contain large concentrations of incompatible elements such as zirconium, hafnium and uranium. Nevertheless, in the Critical Zone of the Bushveld Complex, there are stratiform mafic pegmatoids, with greater concentrations of incompatible elements than the other layered rocks. A number of samples of these mafic pegmatoids were collected, and small zircon separates isolated from the matrix and analysed.

Granitic rocks contain relatively high concentrations of incompatible elements, resulting in greater abundances of zircon, and larger zircon grain size. Granites are also usually fairly rich in uranium, and this may result in the crystallisation U-rich zircons. In these zircons, the release of α-particles and in the decay of uranium and recoil from fission reactions can damage the crystal lattice of the zircons, rendering them more susceptible to chemical weathering. This problem is illustrated by the diverse, disconcordant data available from the Bushveld Complex. For this reason, the two granite samples which were analysed in this study were collected from sites as close to the base of the granite sheet as possible, as these early-formed granites will have formed when the granitic liquid was at its least differentiated, *i.e.* they should have the lowest uranium concentrations, and are therefore likely to be the least affected by radiation damage. (See for example Walraven & Hattingh, 1993)

seen throughout the Kaapvaal Craton at this time, and makes it impossible to date the closure of the Rb-Sr isotopic system in micas, as long periods of elevated temperatures and the presence of hydrothermal fluids could have mobilised Rb, Sr and the ^{87}Sr ion in a K site in the mica lattice for some time after passing through the generally accepted closing temperature. The scatter of mica ages around the preferred age of the Bushveld Complex does however suggest that this alteration phase was contemporaneous with the intrusion.

Complex are a large scale physical manifestation of the presence of significant amounts of hydrothermal fluid around the time of intrusion.

The ages determined using the Rb-Sr method on micas can therefore be interpreted as follows. The errorchron age of 2025±12 Ma determined on all of the mica, plagioclase and whole rock samples is not a true age, but rather the product of intrusion at an earlier stage, probably around 2054Ma, followed by an extended period of high temperature.

The micro-scale investigation of zones of single mica grains indicate a small scale inhomogeneity caused by the alteration event. Hydrothermal alteration can therefore not only reset geochronometers, but can also disturb the internal homogeneity of an isotopic system. If alteration is continues in minerals with very high parent to daughter ratios, the assumption of a single initial radiogenic daughter isotope to invariant daughter isotope ratio may not be strictly valid. The present day $^{87}Sr/^{86}Sr$ ratios are therefore the result of growth of radiogenic ^{87}Sr onto disturbed $^{87}Sr/^{86}Sr$ ratios since the end of the hydrothermal event.

It is of note that model ages determined on mica separates picked from coarsely crushed samples (WV3 Mica, LF-4 Mica, P2-biotite and the two NG-2 samples) lie in the expected range (1991-2044 Ma). The analytical data from these samples represent the average of the micas inside the rock. The anomalously high ages, on the other hand, were determined on parts of large grains in the pegmatoidal rocks, and are believed to represent the local alteration regime within these grains.

To summarise these results, the mica Rb-Sr data from igneous rocks in the Bushveld Complex yield two important results. The Bushveld Complex cooled slowly after initial solidification. This is seen in the general lowering of the mica Rb-Sr age. Around the time of intrusion, an hydrothermal event disturbed the Rb-Sr isotopic systematics of the individual mica grains within the pegmatoidal rocks. This alteration was, in all likelihood, another manifestation of the large scale thermal event which is

2. The other trend is seen as a concentric distribution of elements, resulting from differentiation and fractionation of the liquid during crystallisation. This trend is seen in the results for Si, Na and Cl, although all of these elements' distributions also clearly show the alteration pattern described above.

Petrographic study of this rock indicates that the plagioclase and amphibole formed after the crystallisation of the pyroxene and phlogopite. The inclusion of a plagioclase grain in the large mica analysed suggests that plagioclase may have started to form while the phlogopite was still crystallising. The plagioclase will however have removed Na and the trivalent ions from the melt, explaining their lower concentration towards the rim of the grain. Magnesium and potassium concentrations are relatively constant across the grain, but are decreased in the cross-grain trend mentioned above. These elements therefore indicate an alteration trend. The potassium concentrations (mean K_2O=8.68%) are slightly lower than what would be expected for a phlogopite mica (9-11%), indicating slight chloritisation.

3.6 Explanation of anomalous model ages

The isochron treatment of the data, petrographic investigations and the microprobe analyses indicate slight alteration of the micas. This does not however explain the relatively large (*c.* 150 Ma) variation in ages recorded in this mica study. A simple hydrothermal model can explain the lowering of the age recorded by resetting, but this alone does not account for the older apparent ages (almost 100 Ma older than the intrusion) which have been determined. The hydrothermal fluids related to the intrusion may however have been present for a considerable time after the solidification of the mafic rocks. During this period, some ^{87}Rb in the K sites in the micas will have decayed to ^{87}Sr. The Sr ion is considerably smaller than the Rb ion and has a different charge, and will therefore have easily been mobilised during the post magmatic alteration event. The radiogenic strontium in Rb sites in the micas may therefore have been redistributed on a micro scale, producing local variations in the $^{87}Sr/^{86}Sr$ ratio. The ultramafic pegmatoids common in the critical zone of the Bushveld

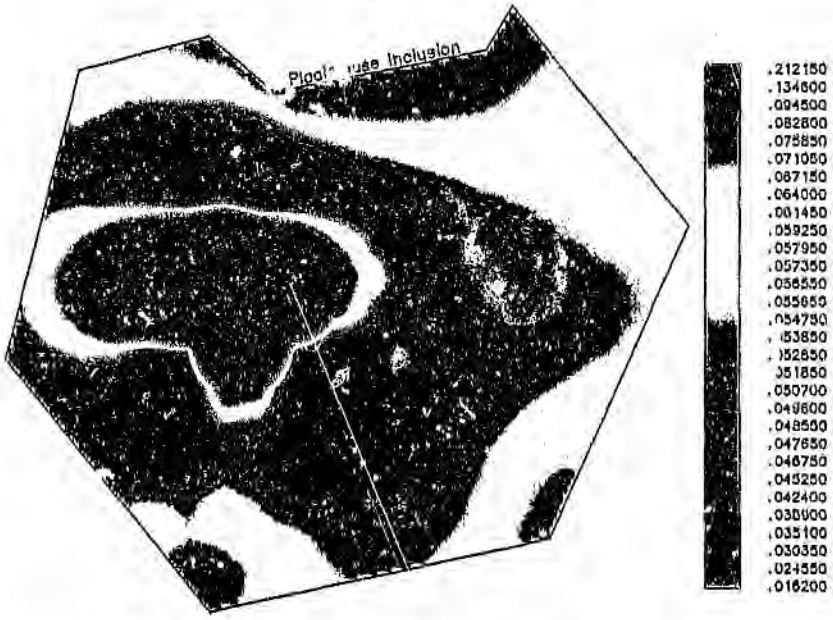

Figure 3.11 Cl ion content of WV2 mica 2

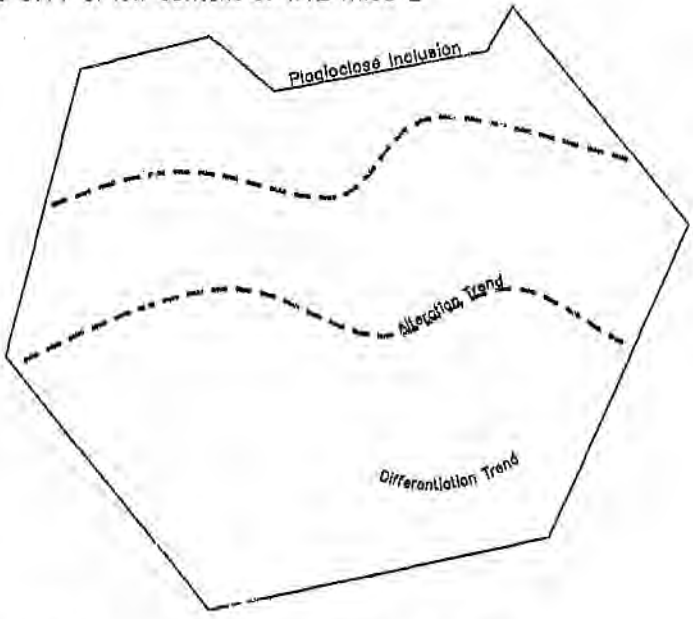

Figure 3.12 Summary of electron microprobe results

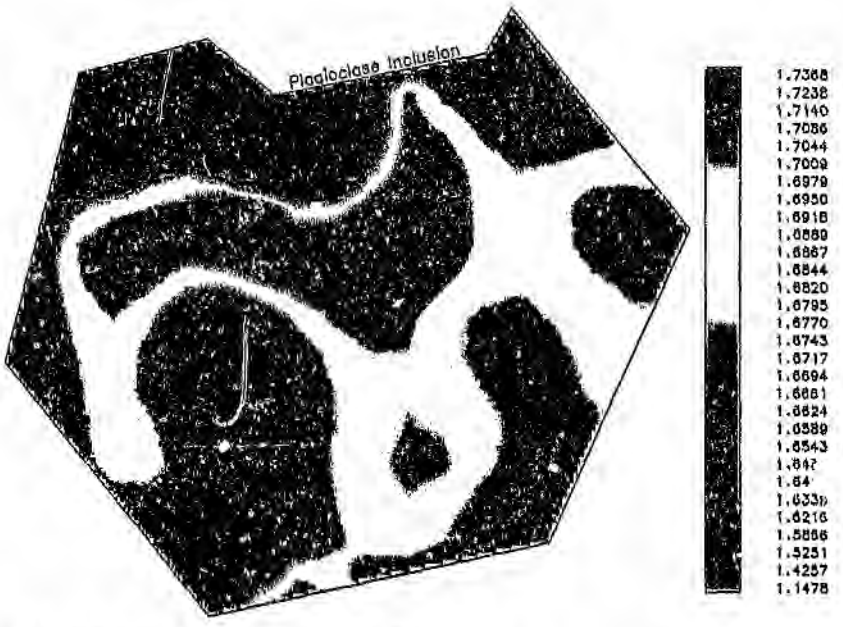

Figure 3.9 K ion contant of WV2 mica 2

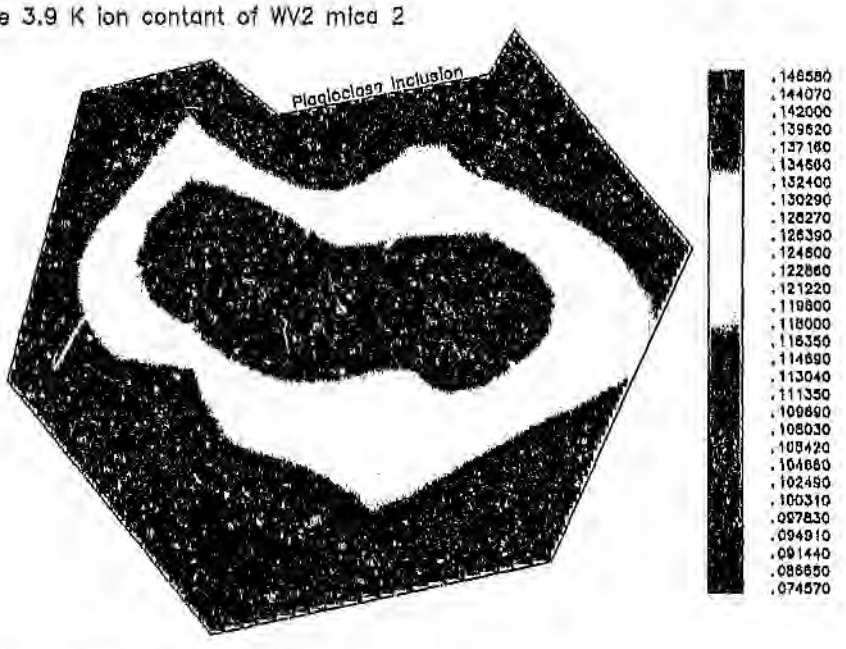

Figure 3.10 Na ion content of WV2 mica 2

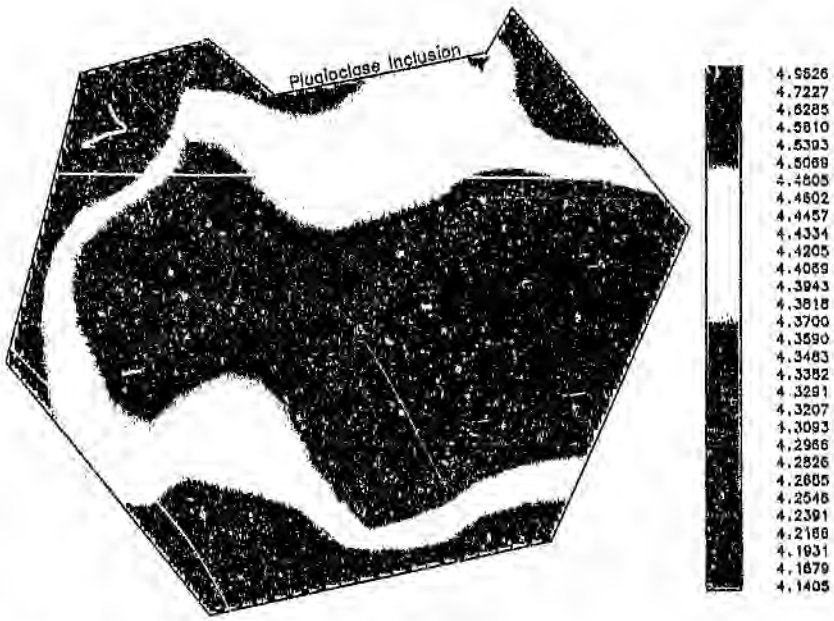

Figure 3.7 Mg ion content of WV2 mica 2

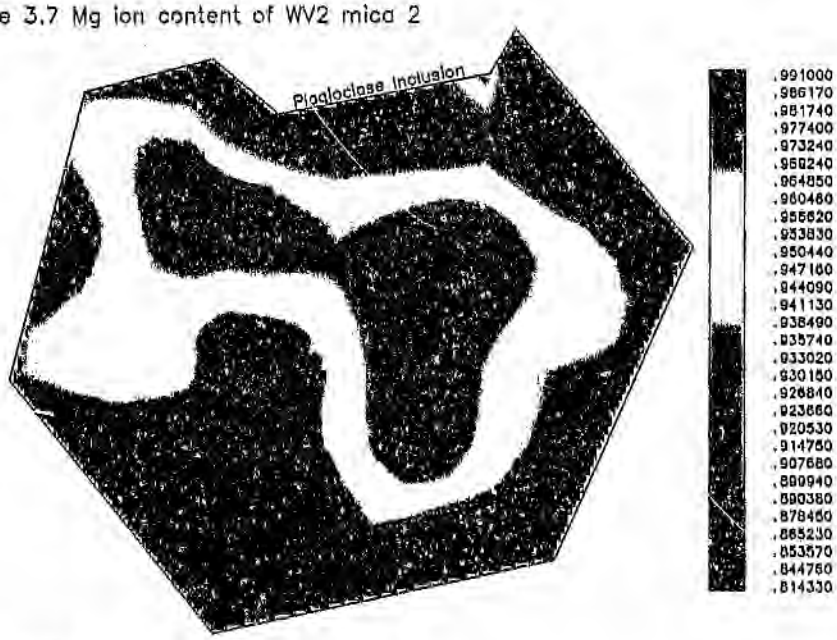

Figure 3.8 Fe ion content of WV2 mica 2

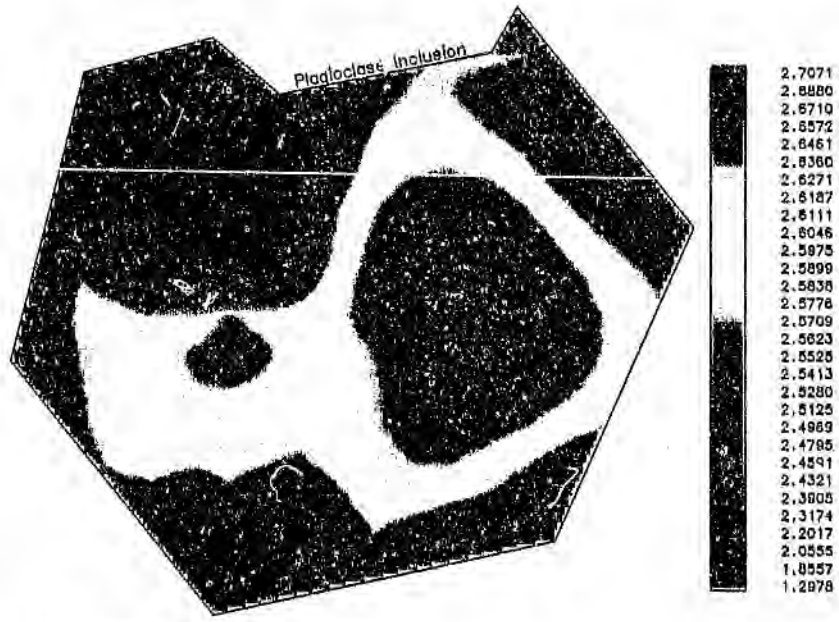

Figure 3.5 Al ion content of WV2 mica 2

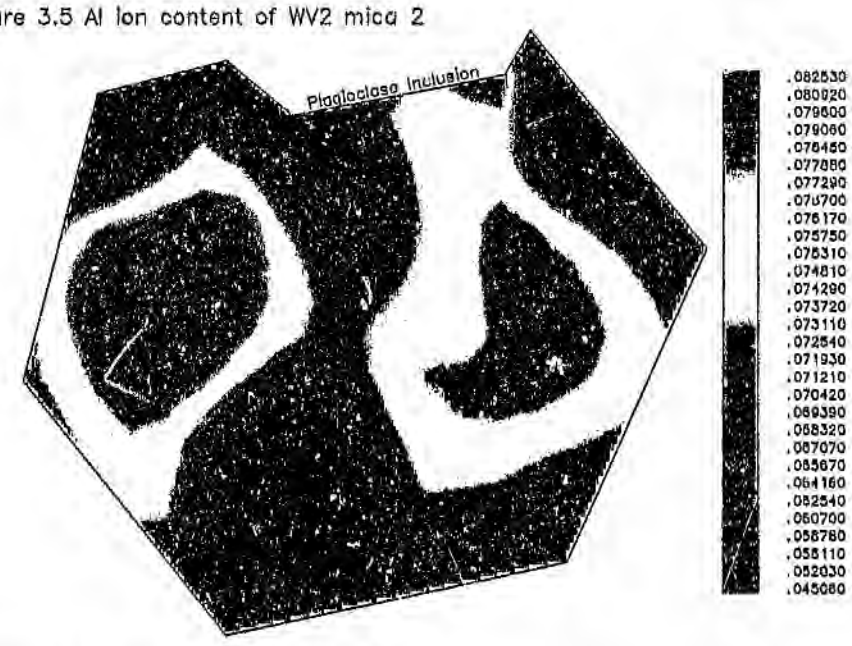

Figure 3.6 Cr ion content of WV2 mica 2

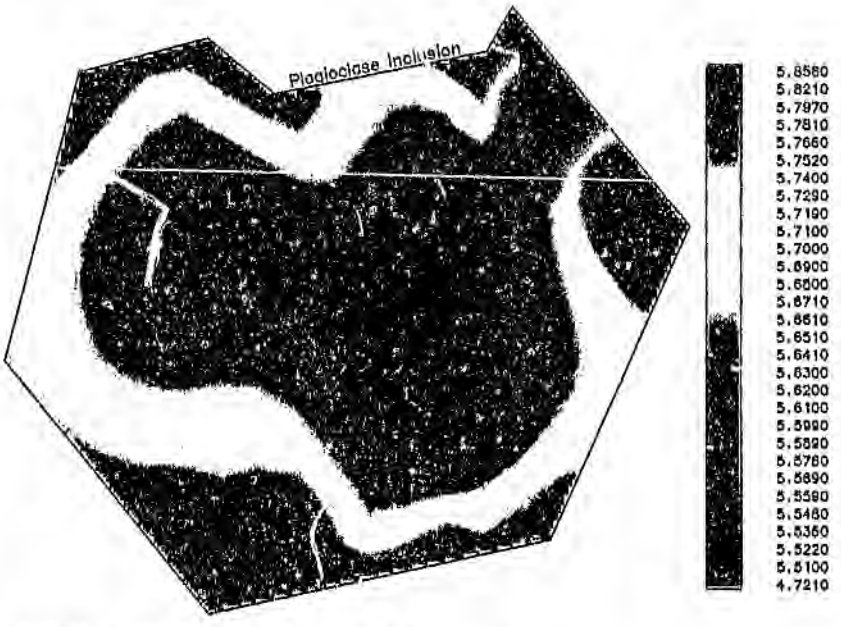

Figure 3.3 Si ion content of WV2 mica 2

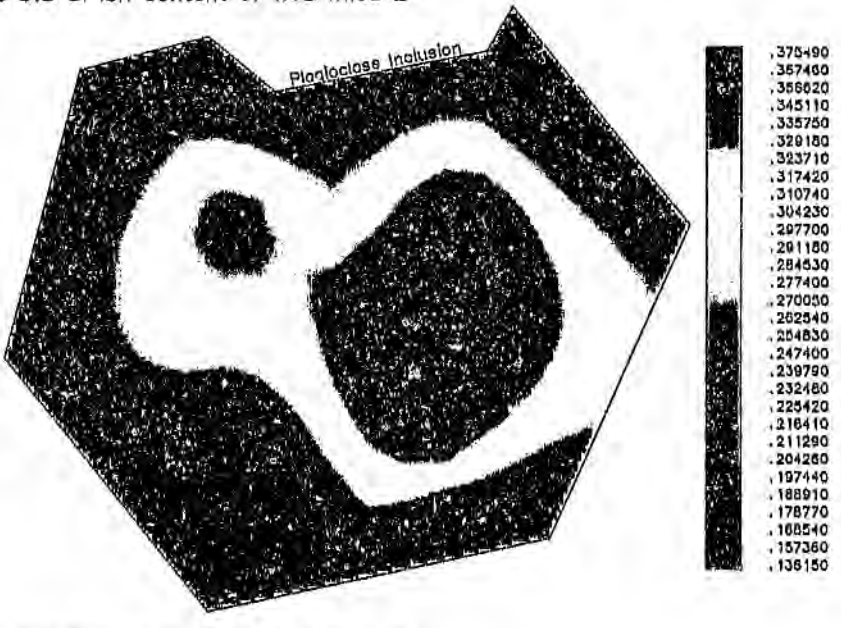

Figure 3.4 Ti ion content of WV2 mica 2

3.5 Electron microprobe study

To investigate these discrepancies, a major element geochemical study was performed using an electron microprobe. Thirty eight analyses were performed on the surface of the grain WV2 Mica 2, on a cleavage face facing the piece which had been isotopically analysed. The ion concentrations on the surface have been gridded using the minimum curvature method of implemented by M Webring of the US Geological Survey (1981). These results are presented graphically in Figures 3.3-3.11 an in tabular form in Appendix 1. The graphical representations were generated using an equal area colour stretch, with Geopak Software. A summary of the results is given in Table 3.2.

Table 3.2 Summary of the results of an electron microprobe study on a cleavage face of mica grain WV2 Mica 2

Ion	Min	Max	Mean	1σ
F	0.0000	0.0586	0.0065	0.0172
Cl	0.0444	0.4770	0.0714	0.0662
Na	0.0604	0.1525	0.1088	0.0245
K	0.6344	1.8068	1.6236	0.1874
Si	0.8759	5.9514	5.5781	0.7632
Ti	0.1175	0.3974	0.2377	0.0820
Al	0.6353	2.7224	2.4392	0.4161
Cr	0.0266	0.0836	0.0674	0.0135
Fe	0.7607	1.0043	0.9098	0.0680
Mg	4.1424	5.6888	4.5078	0.3050
Total	10.7704	16.1454	15.5503	0.8469
Mg/Mg+Fe	0.8073	0.8608	0.8315	0.0165

Two distinct distribution patterns have been observed for these results:

1. One trend cuts across the grain, indicating some form of alteration, with the fluids responsible for the alteration focused along a trend running in this direction. Note that this trend runs subparallel to the plagioclase inclusion inside the grain. This trend is seen most clearly in the results for Al, Cr, Mg, Fe and K.

Across the large grain (WV2 Mica 1), the Rb concentration is relatively constant. The large variation in the $^{87}Sr/^{86}Sr$ ratio therefore can only result from variations in the initial Sr concentration. A likely mechanism for this is the growth of these large mica grains over a period of time, with the outer rims of the grains crystallising after the removal of Sr from the melt by the crystallisation of plagioclase. This is confirmed by the presence of the large plagioclase inclusion observed in WV2 Mica 2.

Model age determinations produce results ranging from 1953-2146Ma. The mean of these model ages is 2035 Ma, with a standard deviation of 50 Ma. These data suggest that the samples are altered, but suggest a more complex process than simply the removal of radiogenic Sr, which would simply have resulted in the lowering of the ages. This process can be invoked to explain the slightly young 2025 Ma age determined by regression on the mica, whole rock and plagioclase data. The error attributable to analytical error is of the order of 20 Ma on each individual sample. This therefore requires a geological process which can produce both older and younger apparent ages in the micas. These data are presented graphically on Figure 3.2.

At grain scale, similar results were recorded. The single grain which was cut and analysed gave results which were not easy to interpret. Using the conventional model of radiogenic Sr loss, it would be expected that the youngest ages would be recorded at the rim of the mica flake, where it would be more susceptible to weathering, and that the oldest ages would be preserved in the centre of the grain. A different pattern was however observed, the oldest age (2119 Ma) being measured at the rim and the youngest (1995 Ma) in the intermediate zone between the core and the rim.

The analyses of the outer rim of the grain also show the largest deviation from the errorchron line. This shows the greater effect of alteration on the outer rim of the grain, that one would reasonably expect for a chloritised mica grain.

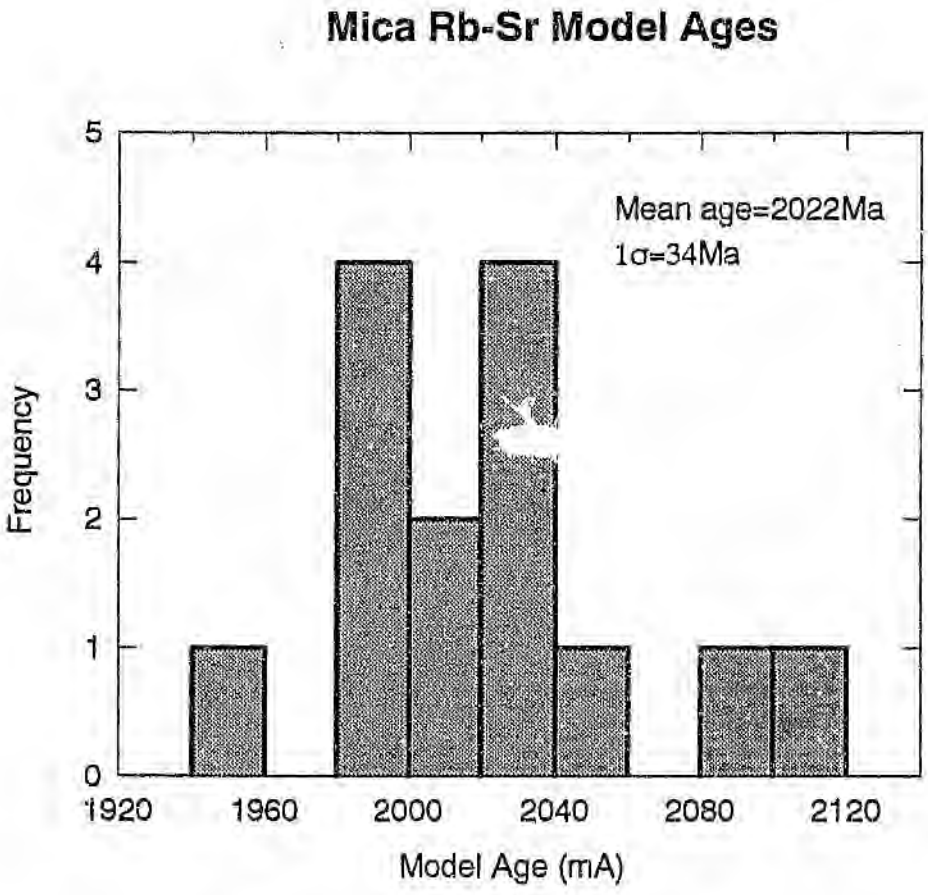

Figure 3.2 Histogram of mica Rb-Sr model ages from the Bushveld Complex.

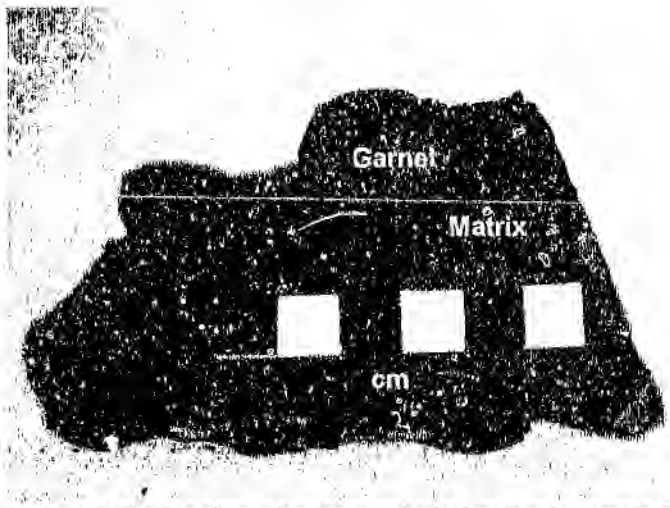

Plate 5.1 Section through a large euhedral garnet in sample GM-1

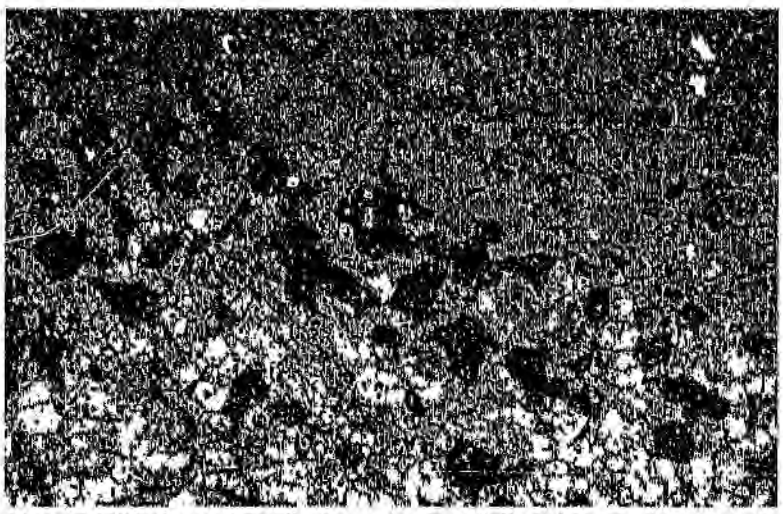

Plate 5.2 Biotite and cordierite grains paralleling the growth zoning in a garnet in sample GM-1 (x200)

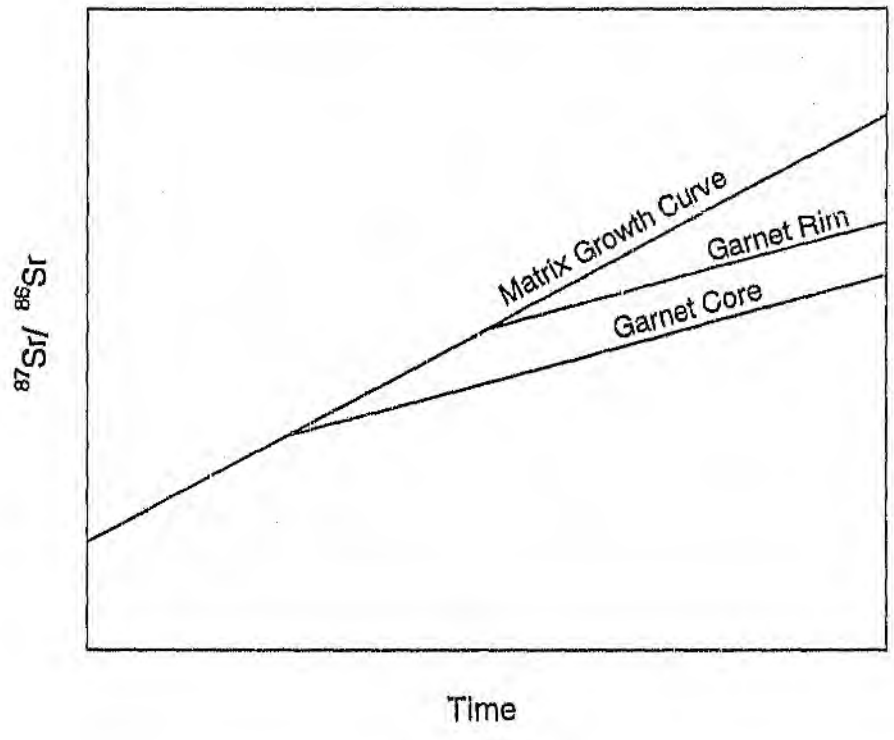

Figure 5.1 Compston Diagram, indicating how Rb-Sr isotopic data can be used to determine the period of growth of a garnet. (After Christensen *et al.*,1989)

for the study. Two adjacent slices were cut through the middle of the grain. One slice was used for the isotopic analysis, and the facing surface on the other slice was analysed using an electron microprobe.

CHAPTER FIVE: Rb-Sr STUDY OF GARNETS FROM THE CONTACT AUREOLE OF THE BUSHVELD COMPLEX

Garnets have very low Rb and Sr concentrations, relative to the pelitic rocks from which they grow. Also, their Rb/Sr ratios are extremely low, relative to their matrix. Because of the very low Rb and Sr concentrations, the Rb/Sr ratio of the rock matrix does not change significantly during garnet growth. In general, pelites have high Rb/Sr ratios, and consequently high $^{87}Rb/^{86}Sr$ ratios. During prolonged metamorphic events, the $^{87}Sr/^{86}Sr$ ratio of the matrix will change because of the decay of ^{87} Rb to ^{87} Sr. Garnets, sampling the Sr in the matrix will record this change in the $^{87}Sr/^{86}Sr$ ratio with time, and because of their low Rb/Sr ratios, should preserve this change (Christensen, *et al.*, 1989). This is analogous to the Sm-Nd model age approach. This effect is shown graphically on a Compston diagram (Fig. 5.1), where the isotopic data are plotted against the age. The lines on the plot therefore represent the growth of the $^{87}Sr/^{86}Sr$ ratio with time. Knowing the age of the rock, it is possible to read off the initial ratio. In this case, the whole rock line is plotted, and the points in the garnet projected back onto this line. Using this technique, it should be possible to determine the difference in age between the two zones of the garnet. This technique can only be used where the source rock has a high Rb/Sr ratio and the mineral (garnet) has a low Rb/Sr ratio and low concentrations of both elements, as only in such a rock will the $^{87}Sr/^{86}Sr$ ratio vary significantly over time, while the Rb/Sr ratio will remain reasonably constant.

In the Eastern Transvaal, near Steelpoort, large garnets occur in the garnet-mica-cor dierite hornfelses of the contact aureole of the Bushveld Complex. The hornfelses have high Rb/Sr ratios, making these rocks ideal for this sort of study. A number of samples were collected on the farm Goudmyn outside Steelpoort, approximately 200m from the contact with the Burgersfort Bulge. The exact distance to the contact is difficult to estimate, as the contact zone is highly weathered in outcrop. These samples contain large numbers of garnets 1-2cm in diameter, with occasional crystals approaching 4cm in diameter. (See Plate 5.1) A garnet 3.5cm in diameter was selected

4.5 Conclusions

Conventional zircon and zircon evaporation studies have indicated discordance in Bushveld zircons, and age determinations yield ages younger than the accepted age of the Complex. Discordance in zircons results from radiogenic lead loss, and is a good indicator of an alteration event or period of alteration some time after the emplacement of the Bushveld Complex. Unfortunately, only two samples were analysed, and these two samples came from localities several hundred kilometres from one another in the Bushveld Complex. It is therefore not possible to plot a discordia curve to determine the date of the alteration. In fact, attempting to plot this curve gives a negative lower intercept age on a concordia diagram. This indicates different Pb loss histories for the two samples. Model ages, $^{207}Pb/^{206}Pb$ ages and concordia model ages display a pattern which would be expected for discordant zircons. Nevertheless, new data on different rocks have produced a highly consistent 2054±1.8 Ma age from the granites (Walraven and Hattingh *op. cit.*). This must be accepted as the age of the last igneous event, and together with the unpublished data of Armstrong, tightly constrains the intrusion of the Bushveld Complex in time.

4.4 The single zircon evaporation technique

A single zircon evaporation study, using zircons from samples MS1 was undertaken, in cooperation with Dr F Walraven of the Geological Survey of South Africa, who performed the analyses. The zircons used were some of the larger grains from the sample, and showed some damage, presumably due to radiation. At the time that the analyses were performed, Dr Walraven was still developing the technique. The data are therefore preliminary. However, later work reported by Walraven and Hattingh (*op. cit.*) appears more reliable, largely due to further development of the technique.

Ages in the range 2008-2070 Ma were recorded, most blocks of data giving ages slightly younger than the now accepted age of 2054Ma (Walraven and Hattingh, *op. cit.*). The large scatter of ages and the generally <2054 Ma ages are believed to be the result of discordance.

Data collected using this technique at the BPI, on the VG354, from the Nebo Granite indicate an age of 2028±50 Ma, which is within error of the accepted age of 2054 Ma. However the large uncertainty is due to open system behaviour in the radiation damaged granitic zircons, which did not give a consistent age at higher temperatures of evaporation. In addition, the zircon evaporation technique was still under development at the time of the study, and analytical procedures on the VG354 were still being tested.

The data of Walraven and Hattingh (*op. cit.*) also illustrate the importance of good sample material, as the zircons analysed in their study appear extremely fresh petrographically, whereas the work reported here and much of the earlier work looked at zircons which did not appear entirely fresh petrographically. Initial experiments with zircon abrasion were conducted, as a means of removing altered zones in zircons, but this work was not completed during the analytical phase of this study.

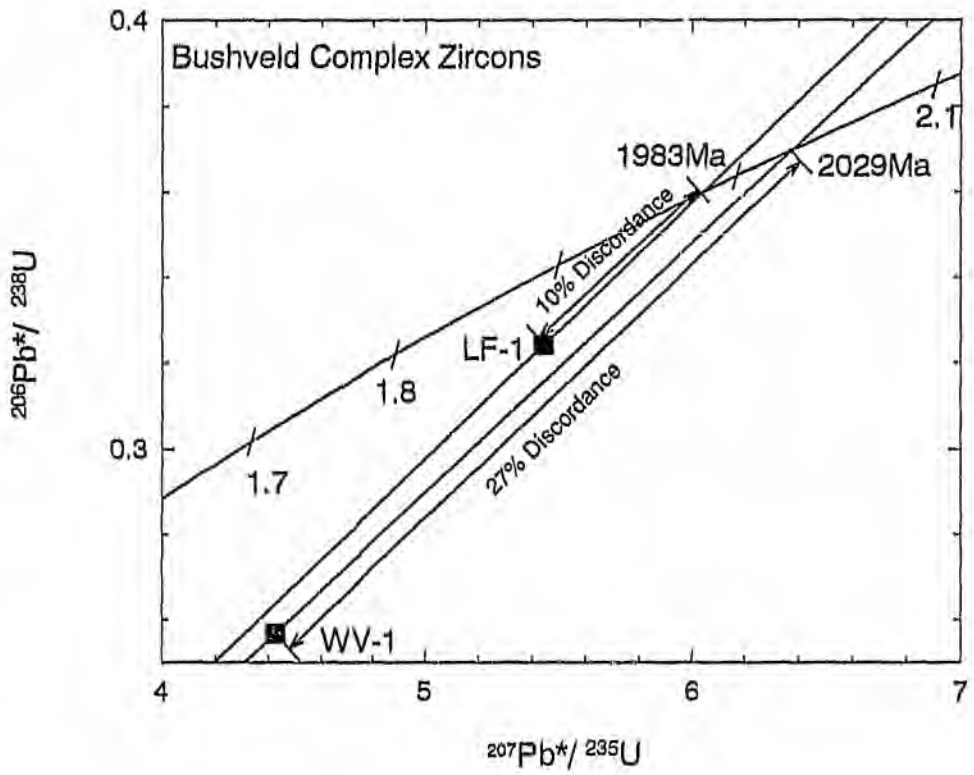

Figure 4.2 Concordia diagram, showing the discordia lines joining data from Bushveld Complex zircons WV-1 and LF-1 to the origin, and the degrees of discordance of these samples.

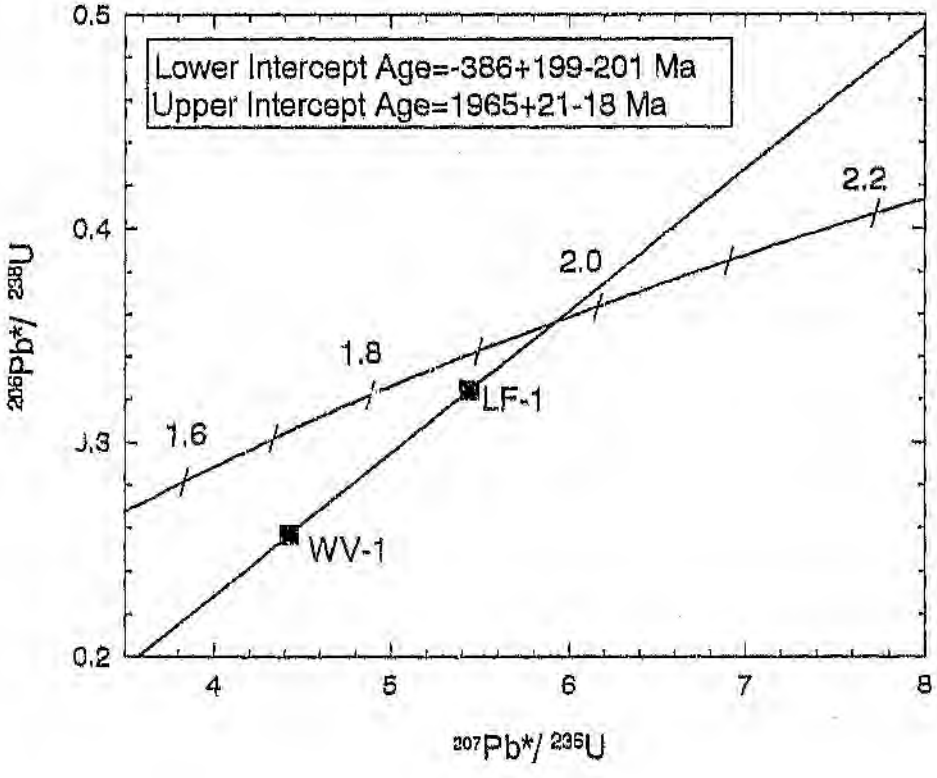

Figure 4.1 Concordia diagram, showing data from Bushveld Complex zircons WV-1 and LF-1

Table 4.2 U-Pb and Pb-Pb age determinations on Bushveld Complex Zircons.

Sample	$^{207}Pb/^{235}U$	t_{235}	$^{206}Pb/^{238}U$	t_{238}	$t_{207/206}$	$t_{concordia}$
WV 1	4.4259	1717 Ma	0.2567	1473 Ma	2029 Ma	2029 Ma
LF1	5.4411	1891 Ma	0.3241	1810 Ma	1983 Ma	1983 Ma
means					2006 Ma	2007 Ma

The low model ages in the sequence $t_{238}<t_{235}<t_{207/206}\leq t_{concordia}$ indicate the expected behaviour for discordant zircons (Eglington & Harmer, *op. cit.*). The degrees of discordance for zircon samples WV1 and LF1 have been calculated at 27% and 10% respectively.

4.3.1 The conventional zircon technique

The conventional zircon technique, as described in Chapter 2, was applied to two zircon samples from the mafic phase of the Bushveld Complex. The samples, WV1 and LF1, were collected from a similar stratigraphic level in the Steelpoort and Brits areas respectively. Uranium-lead isotopic data from these samples are presented in Table 4.1.

Table 4.1 Results of the U-Pb isotopic Study on zircons from the mafic phase of the Bushveld Complex

Sample	U(ppm)	Pb(ppm)	$^{207}Pb/^{235}U$	$^{206}Pb/^{238}U$
WV1	146.60	79.40	4.4259	0.2567
LF1	132.42	79.90	5.4411	0.3241

These data have been used to determine ages using several techniques:

The two samples' data have been plotted on a concordia diagram (Fig. 4.1). This produces an upper intercept age of 1965 +21 -18 Ma, and a lower intercept age of -386 + 199 -201 Ma. The negative or future lower intercept age indicates that the assumption of a linear distribution of samples in U-Pb space (Eglington & Harmer, 1993) is not valid.

Eglington and Harmer (*op. cit.*) suggest two approaches to this problem, viz. the construction of a discordia line which best fits the data and passes through the origin, as suggested by Ludwig (1990) and the calculation of a weighted mean $^{207}Pb/^{206}Pb$ age. Both of these approaches have been applied, and produce indistinguishable ages of 2007 +27 -22 and 2005 +67 -66 Ma respectively. The discordias through the origin and are shown, together with the relevant discordance percentages, on Figure 4.2.

In addition, $^{207}Pb/^{235}U$ and $^{206}Pb/^{238}U$ model ages have been calculated. These and other age data are presented on Table 4.2.

microperthitic feldspar which occur as large anhedral to subhedral grains. A lesser amount of plagioclase is also present. Brown hornblende is the dominant dark mineral, occurring as euhedral to subhedral grains interstitial to the felsic minerals. A small amount of interstitial biotite is also present. Apatite and zircon occur as minor minerals. Small zircons can be seen as an interstitial phase and set into the large interstitial hornblende grains. A few zircons are also found as inclusions in the quartz grains. Zircons separated from this sample are by and large small and app. ir relatively unaltered.

SR1

This sample was collected from an abandoned quarry on the game farm Sable Ranch, about 20km north of Brits. SR1 is a coarse granite consisting dominantly of large anhedral grains of quartz and altered microperthitic K-feldspar, with lesser amounts of plagioclase. The major dark mineral is green hornblende, with inclusions of plagioclase, an opaque mineral and zircon. A significant number of large murky zircons can be seen on the boundaries of the hornblende grains. The zircons separated from this sample are large (some up to 0.5mm in length) and euhedral. They are however cloudy (metamict) due to alteration.

4.3 Analytical Results

Two analytical techniques were used on the zircon samples. The zircon samples from the mafic rocks were analysed using "conventional" wet chemical techniques. U and Pb compositions were determined by isotop n, using the ^{235}U and ^{204}Pb spikes respectively. Pb isotopic compositions were determined from unspiked fractions of the samples. A full description of the analytical technique is given in Chapter 2. Zircons from one of these samples were also analysed using the single grain evaporation technique, also described in Chapter 2.

4.2 Sample Descriptions

4.2.1 Mafic Samples

WV1

A large sample of pegmatitic feldspathic pyroxenite was collected in the Win[illegible] Chromite mine. This sample consists of large (up to 2cm) euhedral crystals of orthopyroxene, and olivine set in a matrix of plagioclase, with minor biotite. The matrix is largely sericitised. Small zircons can be seen in thin section, as inclusions within the pyroxene grains, and a halo of radiation damage can be seen around some of the grains.

LF1

This is a feldspathic pegmatoidal pyroxenite, collected at Lefkochrysos (now Crocodile River) platinum mine. In handspecimen large crystals of orthopyroxene and olivine can be seen in a matrix of plagioclase. In thin section, it is observed that some of the pyroxene grains contain exsolution lamellae of feldspar, and that the margins of the plagioclase grains are eroded by the feldspathic matrix. The matrix appears altered, and a few small zircons can be seen, set in the matrix and in the pyroxene grains. Zircon separates from both of the mafic samples contained few very small, but nonetheless apparently fresh zircons.

4.2.2 Granite Samples

MS1

This sample was collected from a large block of granite blasted during the building of the road from Groblersdal to Jane Furse in Sekhukhuneland. The sample was collected outside the village of Marishane. It is a fresh-looking coarse grained hornblende granite, containing large interlocking quartz and feldspar grains with significant amounts of hornblende. The feldspars are slightly pinkish, and the exposed surfaces of the rock show slight alteration. The dominant minerals are quartz and

Table 5.3 Rb-Sr Isotopic Data from a garnet from the Bushveld Complex Contact Aureole, with GM-1 Rim and GM-1 Int combined to give GM-1 Outer

Sample	Rb	Sr	$^{87}Rb/^{86}Sr$	$^{87}Sr/^{86}Sr$	Preci-sion
Core	2.7990	.6270	1.7602	0.765820	10
Outer	2.6800	19.6700	0.3949	0.727060	420
WR	108.7000	43.7480	7.3434	0.927505	1

Little reliance can be placed on the actual age determined for the whole rock as there are a number of factors which increase the errors and factors such as Sr loss can produce errors which are not easily accounted for. However, the age difference between the zones in the garnet is more robust and more reliance can be placed upon it. Thegarnet growth is assumed to have started very soon after the first input of magma and to have continued for between 13 and 21Ma, but probably in the lower portion of this range. Cooling was also probably quite rapid at first, while the temperature differences between the intrusion and the country rock were large.

5.3 Geothermometry

5.3.1 Method

The method used is that of Ferry & Spear (1978). In a set of experiments it was determined that the partitioning of iron and magnesium into coexisting biotite and garnet follows a regular and predictable pattern, with the proviso that the Mn concentration of both the garnet and the biotite is very low.

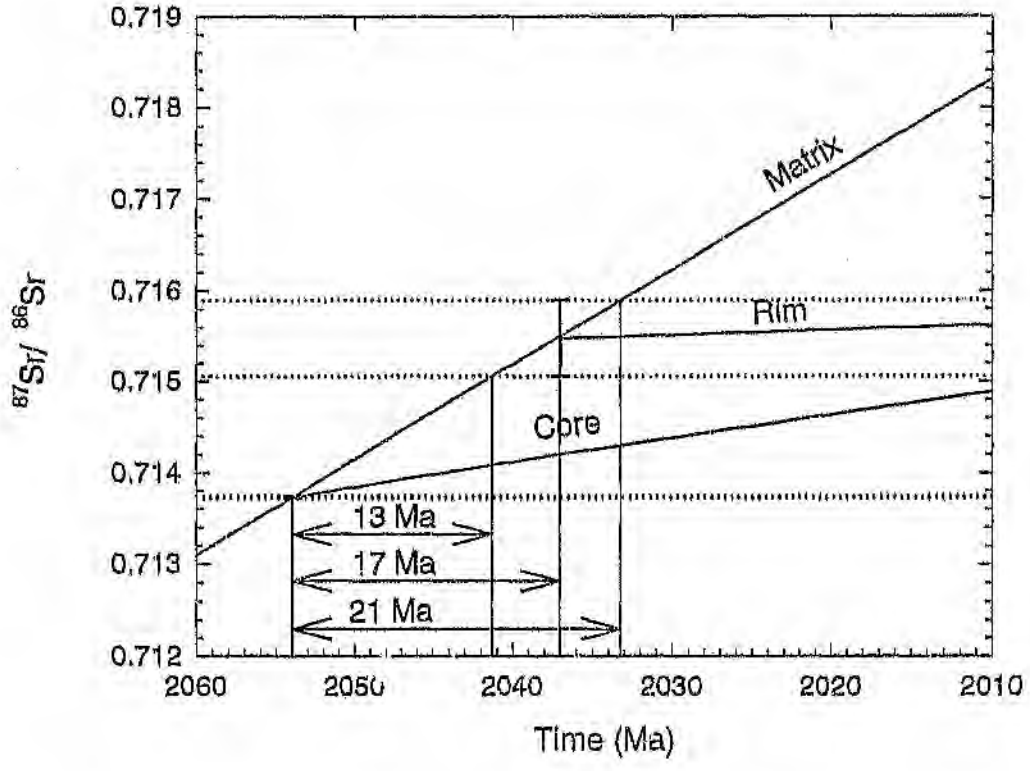

Figure 5.11 Compston Diagram, showing the age difference between the core and outer zones of garnet GM-1.

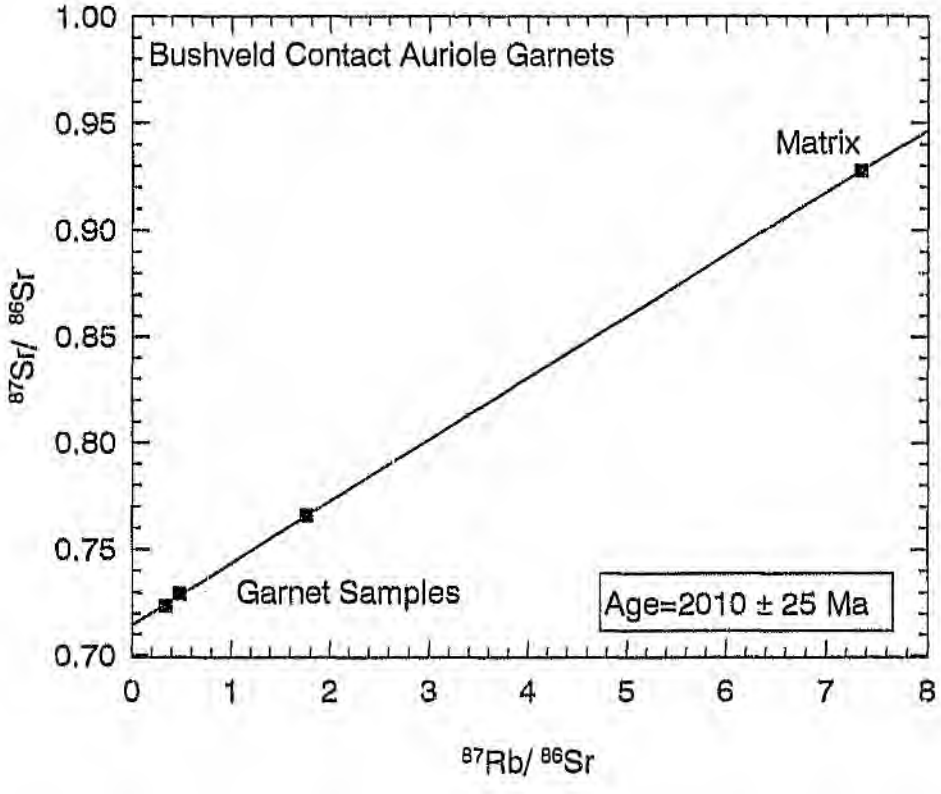

Figure 5.10 Two point isochron diagram for garnet core and matrix from garnet hornfels sample GM-1.

for the sample weight. These data are presented in table 5.2 and on a Compston diagram (see Fig. 5.10). For this diagram, the age of intrusion has been taken as 2054 Ma. It is assumed that the core of the garnet began to grow at this age, and the $^{87}Sr/^{86}Sr$ ratio of the core has been calculated. This ratio will have been the same as that in the whole rock, as no fractionation of this ratio is expected in metamorphic processes. The whole rock curve is then constructed using the present day $^{87}Sr/^{86}Sr$ ratio and this value. Present day data for the rim of the garnet are then back projected until the growth curve intersects that of the matrix. From this diagram it can be seen that the total elapsed time between the intrusion of the Bushveld Complex and the end of garnet growth is of the order of 17 Ma, with the relatively large uncertainty in the $^{87}Sr/^{86}Sr$ ratio of the garnet rim giving a 95% confidence range of 13-21 Ma. This extended period of growth indicates an extended cooling period for the Bushveld Complex. The difference in slope between the two samples' growth curves is a consequence of the small but noticeable amount of mica included in the garnet crystals. While every attempt has been made to remove this contamination, it is not possible to remove submicroscopic grains of mica. It is further assumed that these micas formed at the same time as the garnet zone where they are found.

5.2.1 Mineral Separation

A slice 5mm wide was cut from the middle of the garnet was cut using a thin saw This was stuck to a piece of wide adhesive tape and shattered using a hammer. Fragments were picked from this tape, representative of the three zones. Separation of the garnets from the mica, cordierite and other porphyroblast minerals was effected using heavy liquids and hand picking. These methods are discussed in detail in chapter 2.

Table 5.2 Rb-Sr Isotopic Data from a garnet from the Bushveld Complex Contact Aureole

Sample	Rb	Sr	$^{87}Rb/^{86}Sr$	$^{87}Sr/^{86}Sr$	Precision
GM1Core	2.7990	4.6270	1.7602	0.765820	10
GM1 Int	2.3130	14.1400	0.4743	0.729346	400
GM1 Rim	3.2560	28.3600	0.3327	0.723466	18
GM-1 WR	108.7000	43.7480	7.3434	0.927505	1

The emplacement age has been calculated from these data by fitting a two point line through the results from the rim of the garnet and the whole rock on an isochron diagram. This should yield a model age closest to the age of emplacement of the Bushveld Complex, assuming that the Rb-Sr isotopic system was totally reset in the original shale by the metamorphism. An age of 2010±25 Ma is thus determined (see Fig. 5.9), which is slightly younger than the preferred age of 2054 Ma for the Bushveld Complex. This indicates that the metamorphic and subsequent processes in this rock have reset the age of the garnet hornfels, to an age younger than the true age of metamorphism.

5.2.2 Interpretation

The microprobe study has shown that the rim and intermediate zone are in fact a single zone, there being no sharp chemical division between them. The data for these two zones were combined by calculating average values, after weighting each data set

1. Mn, Mg and Fe follow a smooth pattern through the grain, with Fe and Mn contents decreasing outwards from the centre of the grain, and Mg content increasing outwards. This is indicative of growth of a garnet under changing P-T conditions, most likely decreasing temperature with time.

2. Al, Ti and Ca have a more complex distribution, Ti and Ca contents decreasing from the centre into an intermediate zone and then increasing, and Al increasing and then decreasing and increasing again. This distribution suggests zoning, with at least two distinct periods of growth.

3. The Si content of the garnet appears relatively constant across the grain.

4. Unlike the mica discussed in Chapter 3, no major cross-cutting geochemical trends have been observed in these data These probe data therefore indicate that the garnet grew from the centre outwards, and has not been influenced by any outside effects, which will disturb this pattern. This garnet is therefore ideal for the isotopic study described below.

5.2 Rb-Sr Isotope study

The garnets have three petrographically discernible zones, a thin outer rim rich in plagioclase, quartz and cordierite inclusions, an intermediate zone, with fewer large cordierite and biotite inclusions and a central zone, highly fractured, again with cordierite and biotite (See Plate 5.2). The intermediate and central zones are separated by a clear break, suggesting that there may have been a break in garnet growth, possibly between two successive intrusive events. The three zones and the mica rich matrix were all analysed.

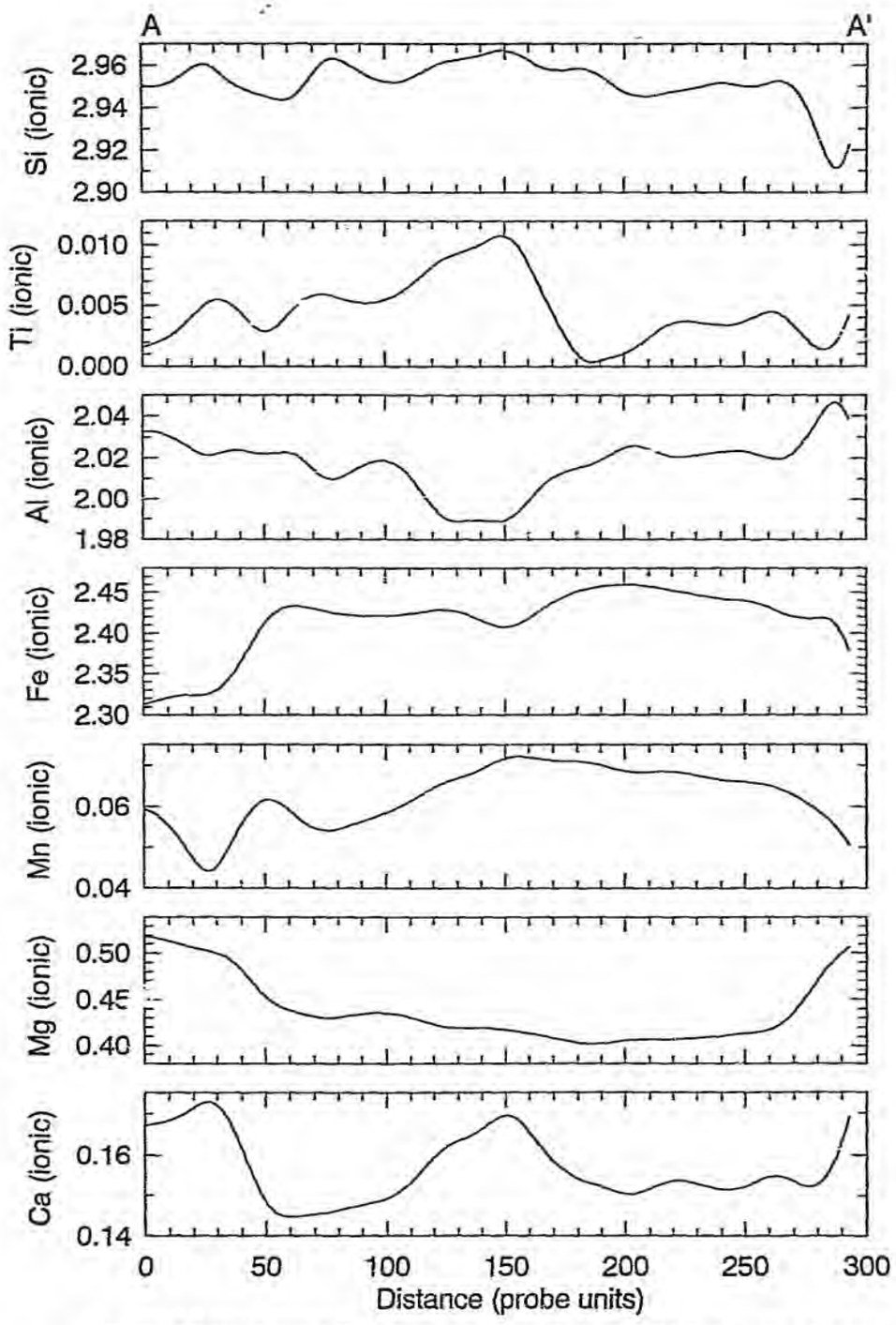

Figure 5.9 Geochemical X-sections across garnet sample GM-1 along line A-A' (see Figs 5.2-5.8).

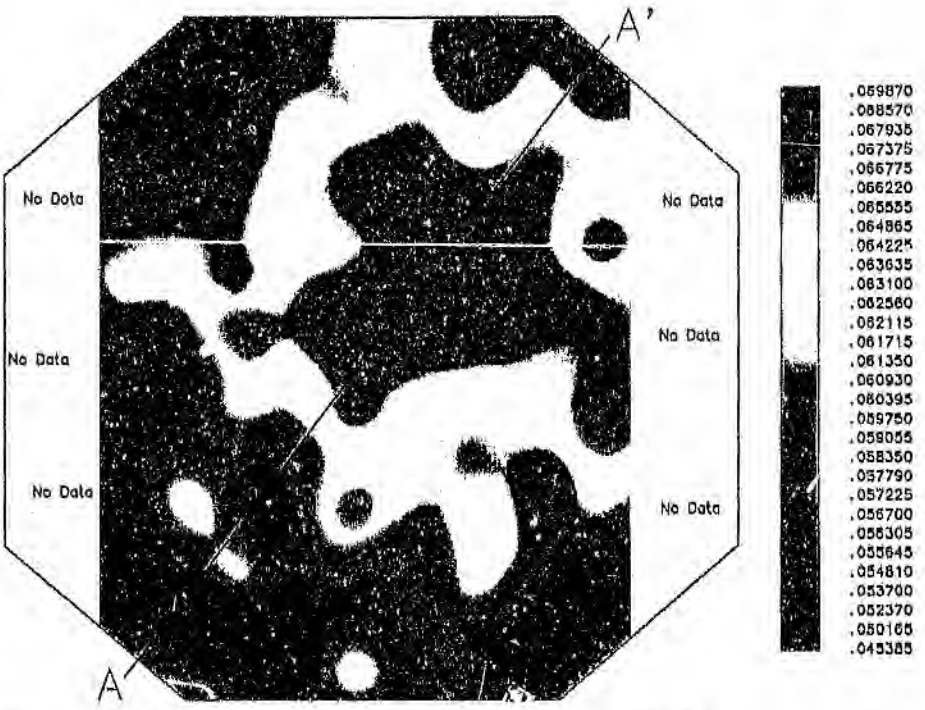

Figure 5.8 Mn ion content across garnet GM1

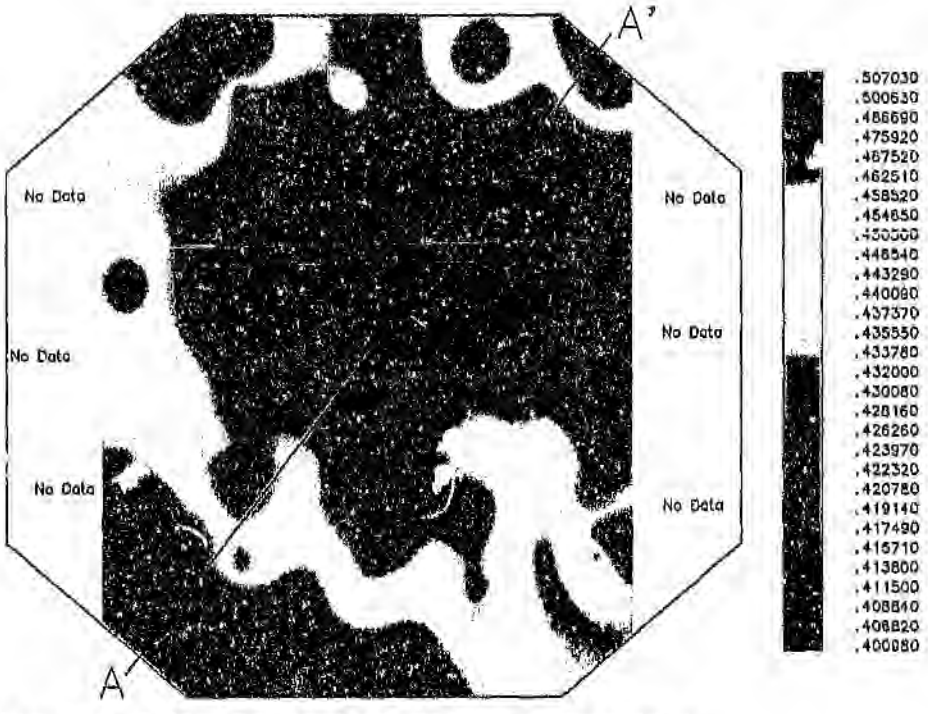

Figure 5.6 Mg ion content across garnet GM1

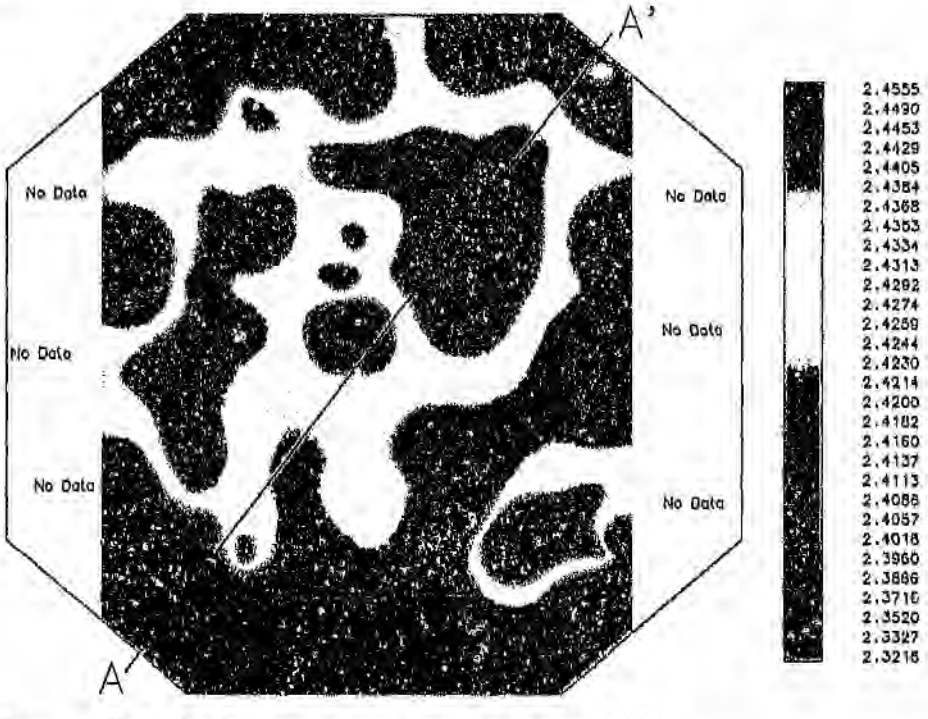

Figure 5.7 Fe ion content across garnet GM1

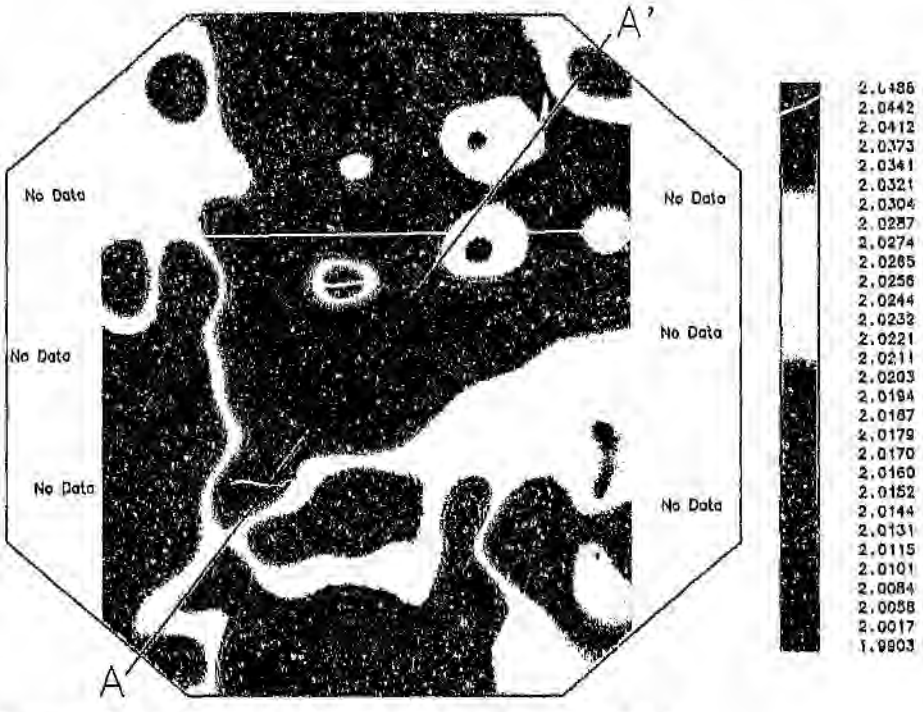

Figure 5.4 Al ion content across garnet GM1

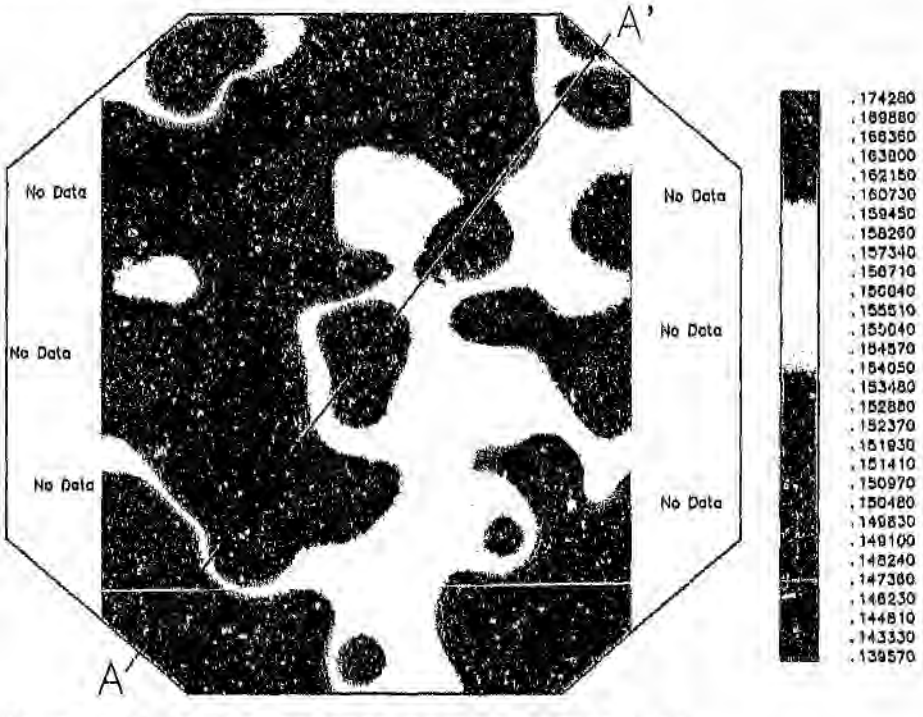

Figure 5.5 Ca ion content across garnet GM1

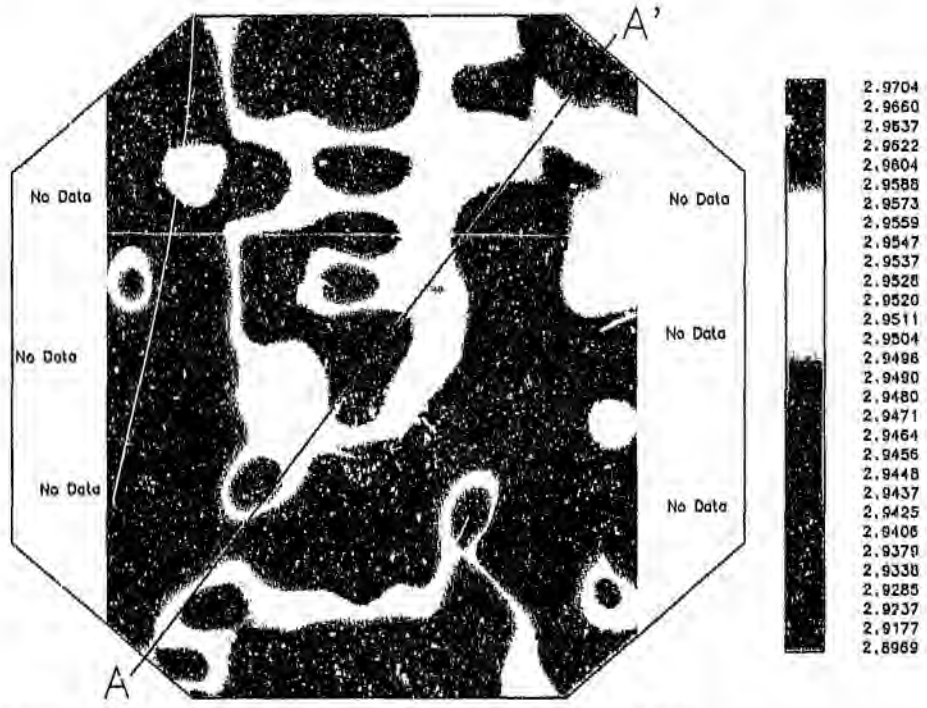

Figure 5.2. Si ion content across garnet GM1

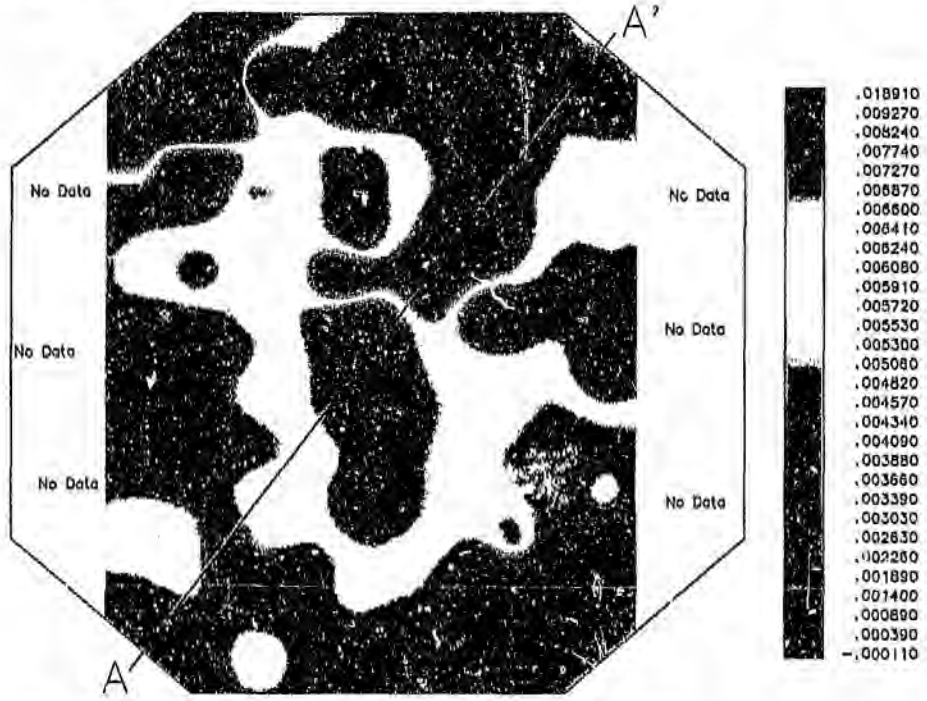

Figure 5.3 Ti ion content across garnet GM1

Petrographic investigations (see Plate 5.2) of the garnets indicate clear growth zoning, which may be related to stages in the development of the Bushveld Complex, possibly even to major injections of magma. The earliest intrusions in thebulge may have caused the first zone of growth, with the rest of the intrusion causing the second. The garnets are filled with inclusions of plagioclase, quartz, cordierite and biotite. For the technique described above, the biotite poses a problem, as the high Rb/Sr ratio in the biotite will produce a highly radiogenic $^{87}Sr/^{86}Sr$ ratio. The biotite must therefore be removed from the samples b fore they can be analysed.

5.1 Microprobe analyses

The microprobe analyses revealed that the garnet followed a simple growth path, most elements being distributed radially about the centre of the grain. These data are shown graphically on figures 5.2-5.8 and summarised in Table 5.1, and are presented in full in Appendix 2. Figure 5.9 shows geochemical sections through the garnet along section line A-A'.

Table 5.1 Summary of electron microprobe data across a section through garnet GM-1

Ion	Max	Min	Mean	1σ
Si	2.8421	2.9870	2.9470	0.0262
Ti	0.0000	0.0660	0.0055	0.0091
Al	1.9792	2.0825	2.0232	0.0217
Fe	2.2501	2.5074	2.4105	0.0455
Mn	0.0421	0.0764	0.0602	0.0079
Mg	0.3957	0.5448	0.4464	0.0382
Ca	0.1305	0.1917	0.1553	0.0128
Total	8.0217	8.1232	8.0482	0.0214

The following trends are observed in these data (These trends are indicated on Figure: 5.9):

Allsopp, H. L., Fitch, F. J., Miller, J. A. and Reimold, W. U., 1991, $^{40}Ar/^{39}Ar$ stepheating age determinations relevant to the formation of the Vredefort Dome, South Africa: *S. Afr. J. Sci.*, 87(9), 431-442.

Ballhaus, C. G. and Stumpfl, E. F., 1985, Fluid inclusions in the Merensky and Bastard Reefs, western Bushveld Complex: *The Canadian Mineralogist*, 23 (part 2), 294.

Barton, J. M. j. r., Cawthorn, R. G. and White, J., 1986, The role of contamination in the evolution of the Platreef of the Bushveld Complex.: *Econ. Geol.*, 81, 1096-1104.

Burger, A. J. and Coertze, F. J., 1973, Radiometric age measurements on rocks from southern Africa to the end of 1971: *Geol. Surv. S. Afr. Bull. 58*, 46pp.

Burke E E (ed), 1969, *The Journals of Carl Mauch, His travels in the Transvaal and Rhodesia*, 1869-1872. National Archives of Rhodesia, 314pp.

Cawthorn, R. G. and Poulton, K. L., 1987, Evidence for fluid in the footwall beneath potholes in the Merensky Reef of the Bushveld Complex: In: Prichard H. M., Potts P.J., Bowles J. F. W., Cribb S. J., 1987, *Geo-Platinum 87*, Dep. of Earth Science, Milton Keynes, United Kingdom, 343-356.

Cawthorn, R. G., Meyer, P. S. and Kruger, F. J., 1991, Major addition of magma at the Pyroxenite Marker in the western Bushveld Complex, South Africa: J. Petrol., 32 (4), 739-763.

x	y	Si	Ti	Al	Fe	Mn	Mg	Ca	Total
330	329	2.92	0.07	2.05	2.35	0.04	0.51	0.18	8.12
306	250	2.96	0.01	2.00	2.37	0.06	0.48	0.15	8.04
349	250	2.96	0.01	2.01	2.43	0.06	0.41	0.15	8.03
389	250	2.93	0.00	2.05	2.45	0.07	0.42	0.14	8.06
427	250	2.96	0.00	2.02	2.46	0.07	0.40	0.15	8.06
482	250	2.95	0.01	2.01	2.42	0.07	0.42	0.16	8.04
493	150	2.90	0.00	2.06	2.41	0.05	0.53	0.13	8.08
454	150	2.84	0.01	2.08	2.51	0.06	0.45	0.17	8.12
407	150	2.94	0.01	2.03	2.42	0.06	0.42	0.16	8.04
357	150	2.92	0.01	2.05	2.43	0.05	0.45	0.15	8.06
315	150	2.89	0.01	2.05	2.38	0.05	0.52	0.19	8.09

APPENDIX 2. ELECTRON MICROPROBE DATA FROM A SECTION THROUGH GARNET GRAIN GM-1 (AS IONIC PROPORTIONS)

x	y	Si	Ti	Al	Fe	Mn	Mg	Ca	Total
489	347	2.95	0.01	2.02	2.32	0.05	0.51	0.18	8.04
490	335	2.89	0.00	2.06	2.43	0.06	0.50	0.15	8.09
489	322	2.95	0.00	2.03	2.39	0.06	0.47	0.15	8.05
489	268	2.95	0.01	2.02	2.40	0.06	0.42	0.16	8.03
489	216	2.95	0.01	2.03	2.40	0.07	0.42	0.17	8.04
488	196	2.95	0.01	2.02	2.41	0.07	0.42	0.16	8.04
489	168	2.94	0.01	2.02	2.44	0.06	0.42	0.16	8.05
489	147	2.95	0.00	2.02	2.45	0.06	0.43	0.15	8.05
489	132	2.96	0.00	2.03	2.39	0.05	0.45	0.15	8.03
440	339	2.95	0.00	2.02	2.39	0.06	0.49	0.15	8.06
440	332	2.94	0.00	2.01	2.41	0.06	0.47	0.15	8.05
440	306	2.96	0.00	2.03	2.44	0.06	0.42	0.14	8.05
440	264	2.94	0.00	2.04	2.47	0.07	0.41	0.15	8.06
440	239	2.95	0.01	2.00	2.45	0.07	0.40	0.17	8.04
440	160	2.98	0.01	2.00	2.39	0.06	0.42	0.16	8.02
440	136	2.97	0.00	2.00	2.42	0.06	0.43	0.15	8.04
440	120	2.97	0.00	2.01	2.41	0.06	0.44	0.14	8.03
395	105	2.99	0.00	2.01	2.33	0.07	0.48	0.15	8.02
395	126	2.95	0.01	2.02	2.42	0.06	0.44	0.16	8.04
395	162	2.92	0.01	2.05	2.44	0.07	0.41	0.15	8.06
395	205	2.97	0.01	1.98	2.43	0.07	0.41	0.17	8.04
395	235	2.98	0.01	1.98	2.39	0.08	0.42	0.16	8.03
395	266	2.97	0.01	2.00	2.42	0.07	0.41	0.16	8.03
395	297	2.94	0.01	2.02	2.45	0.07	0.40	0.16	8.06
350	329	2.97	0.00	2.00	2.42	0.06	0.43	0.15	8.03
350	335	2.97	0.01	2.01	2.34	0.05	0.49	0.17	8.02
395	322	2.98	0.00	2.00	2.40	0.06	0.44	0.15	8.04
350	287	2.94	0.01	2.02	2.44	0.06	0.43	0.15	8.05
350	266	2.96	0.01	1.99	2.46	0.06	0.41	0.15	8.04
350	237	2.96	0.01	2.00	2.44	0.07	0.41	0.15	8.04
350	208	2.96	0.01	2.01	2.43	0.06	0.43	0.14	8.04
350	171	2.97	0.01	2.00	2.43	0.05	0.42	0.14	8.03
350	142	2.95	0.00	2.01	2.44	0.06	0.43	0.14	8.04
350	102	2.96	0.01	2.00	2.33	0.04	0.50	0.18	8.03
330	96	2.96	0.00	2.03	2.25	0.00	0.54	0.16	8.02
331	100	2.95	0.00	2.04	2.35	0.05	0.50	0.16	.06
331	128	2.97	0.01	2.02	2.32	0.04	0.50	0.17	8.03
330	144	2.94	0.01	2.03	2.36	0.06	0.49	0.17	8.05
330	167	2.92	0.00	2.04	2.43	0.07	0.46	0.15	8.06
330	188	2.92	0.00	2.06	2.46	0.06	0.44	0.14	8.07
330	221	2.92	0.00	2.04	2.46	0.06	0.44	0.15	8.07
330	250	2.91	0.01	2.07	2.44	0.06	0.41	0.16	8.06
330	297	2.96	0.00	2.03	2.44	0.05	0.44	0.13	8.04

APPENDIX 1. ELECTRON MICROPROBE DATA FROM A CLEAVAGE FACE OF MICA GRAIN WV2 MICA 2 (AS IONIC PROPORTIONS)

x	y	F	Cl	Na	K	Si	Ti	Al	Cr	Fe	Mg	Total	Mg/ Mg+Fe
397	341	0.05	0.09	0.08	1.63	5.86	0.15	2.39	0.06	0.85	4.62	15.76	0.85
307	322	0.05	0.05	0.09	1.65	5.86	0.15	2.39	0.06	0.76	4.70	15.77	0.86
307	472	0.00	0.07	0.09	1.54	5.85	0.14	2.35	0.06	0.82	4.82	15.73	0.85
307	430	0.00	0.05	0.14	1.76	5.51	0.34	0.64	0.08	0.98	4.36	13.86	0.82
307	400	0.05	0.48	0.14	1.61	5.59	0.31	2.65	0.08	0.92	4.30	16.15	0.82
307	370	0.00	0.05	0.12	1.63	5.73	0.21	2.57	0.06	0.93	4.44	15.74	0.83
307	348	0.00	0.06	0.09	1.65	5.76	0.17	2.56	0.07	0.84	4.55	15.75	0.84
275	390	0.00	0.06	0.11	1.69	5.67	0.25	2.57	0.08	0.96	4.37	15.76	0.82
300	390	0.00	0.05	0.12	1.63	5.62	0.30	2.64	0.08	0.94	4.33	15.71	0.82
330	390	0.08	0.05	0.14	1.66	5.61	0.31	2.60	0.07	0.92	4.34	15.75	0.83
361	390	0.00	0.05	0.13	1.70	5.50	0.40	2.66	0.08	0.99	4.26	15.77	0.81
388	390	0.00	0.05	0.13	1.66	5.67	0.35	2.72	0.08	0.94	4.16	15.67	0.81
406	457	0.00	0.06	0.08	1.64	5.85	0.14	2.43	0.04	0.83	4.67	15.75	0.85
375	457	0.00	0.07	0.10	1.64	5.67	0.27	2.61	0.08	0.93	4.48	15.75	0.83
349	457	0.00	0.06	0.11	1.68	5.66	0.23	2.55	0.07	0.91	4.47	15.78	0.83
325	457	0.00	0.09	0.07	0.63	5.85	0.19	2.41	0.05	0.88	4.54	14.72	0.84
300	457	0.00	0.06	0.13	1.68	5.66	0.25	2.60	0.07	0.97	4.34	15.76	0.82
274	457	0.00	0.07	0.07	1.33	5.82	0.13	0.86	0.05	0.95	5.69	14.96	0.86
383	470	0.00	0.09	0.08	1.68	5.74	0.21	2.68	0.08	0.99	4.33	15.76	0.81
390	470	0.00	0.08	0.11	1.67	5.74	0.18	2.67	0.06	0.86	4.53	15.80	0.84
395	470	0.00	0.07	0.08	1.60	0.88	0.17	2.29	0.05	0.83	4.81	10.77	0.85
290	341	0.00	0.07	0.09	1.61	5.84	0.17	2.44	0.07	0.79	4.62	15.70	0.85
327	341	0.00	0.05	0.09	1.62	5.91	0.14	2.39	0.03	0.81	4.65	15.70	0.85
350	341	0.00	0.05	0.11	1.69	5.67	0.26	2.58	0.07	0.92	4.36	15.73	0.83
375	341	0.00	0.05	0.10	1.65	5.72	0.19	2.53	0.07	0.88	4.57	15.77	0.84
350	330	0.00	0.05	0.09	1.66	5.82	0.16	2.49	0.05	0.78	4.72	15.77	0.86
325	330	0.00	0.06	0.11	1.69	5.73	0.18	2.62	0.07	0.89	4.60	15.84	0.84
300	330	0.00	0.04	0.06	1.20	5.95	0.12	1.88	0.04	0.93	5.50	15.72	0.86
386	477	0.00	0.09	0.09	1.66	5.72	0.19	2.48	0.06	0.89	4.63	15.80	0.84
406	425	0.00	0.06	0.12	1.72	5.72	0.28	2.57	0.08	0.96	4.21	15.71	0.82
375	425	0.00	0.05	0.14	1.68	5.47	0.38	2.71	0.08	1.00	4.26	15.78	0.81
342	425	0.00	0.05	0.13	1.71	5.63	0.28	2.58	0.07	0.97	4.38	15.80	0.82
320	425	0.00	0.06	0.15	1.81	5.56	0.34	2.56	0.07	1.00	4.33	15.83	0.81
295	425	0.00	0.05	0.14	1.68	5.56	0.31	2.72	0.08	1.00	4.19	15.74	0.81
268	425	0.00	0.06	0.12	1.70	5.70	0.21	2.58	0.08	0.91	4.41	15.76	0.83
370	335	0.05	0.06	0.09	1.67	5.85	0.14	2.45	0.06	0.82	4.57	15.75	0.85
370	364	0.00	0.05	0.12	1.71	5.55	0.35	2.65	0.07	0.98	4.24	15.72	0.81
370	398	0.00	0.05	0.16	1.68	5.53	0.38	2.71	0.08	0.99	4.14	15.71	0.81
370	430	0.00	0.05	0.13	1.73	5.47	0.36	2.67	0.08	0.99	4.35	15.85	0.81
370	460	0.00	0.08	0.11	1.67	5.69	0.24	2.57	0.08	0.90	4.46	15.80	0.83

The Bushveld Complex can therefore only be fully understood, if it is viewed from a cratonic perspective, and the events leading to the current nature and disposition of the rocks are viewed as a series of events happening over a measurable time period, rather than as a single intrusive event.

6.4 Conclusions

Using a variety of isotopic techniques, it has been possible to date different stages in the early post-emplacement history of the Bushveld Complex. These can then be placed in the context of the development of the Kaapvaal Craton in late Vaalian and early Mokolian times. The Bushveld Complex cooled far more slowly than would be expected from simple convective cooling, indicating that an external heat source must have been present at this time. Evidence for this period of high heat flow is seen throughout the craton, in pervasive thermal overprinting of the isotopic and palaeomagnetic systems.

A time constraint has been placed on the early structural history of the complex. Palaeomagnetic results show that the Bushveld Complex was emplaced in an horizontal attitude, and cooled to below the Curie Temperature for magnetite before thermal relaxation and deformation to it's present centripetally dipping configuration. Geochronological and geothermometric results on garnets from the contact aureole of the Bushveld Complex show that the cooling to below the Curie Temperature took at least 13Ma, and could have taken more than 20Ma.

Rb-Sr isotopic data on micas from the Bushveld Complex show that the effects of pervasive hydrothermal alteration, and place a further time constraint on the cooling of the complex. These data point towards a ±30Ma period until the mafic rocks cooled to below 400°C, and together with $^{40}Ar/^{39}Ar$ results, help document the first 44Ma of the thermal history of the Bushveld Complex.

Various workers (see Chapter 1) have determined ages in this range for events and intrusions on the entire Kaapvaal Craton. Most significant are the ages determined for the Phalaborwa Complex and the Vredefort Dome, and the overprint ages on the Onverwacht Group in the Barberton Mountainland (Weis & Wasserburg, 1987). Resetting of the magnetic orientation in rocks is also recorded in the Witwatersrand Supergroup at this age (Layer *et al.*,1988). This is clearly indicative of a far larger event than the simple intrusion of a mafic complex, even one the size of the Bushveld Complex.

Other studies (for example Cawthorn & Poulton, 1987) and the petrographic studies of the rocks used in this study indicate that significant fluid flow occurred within the complex during and after its intrusion. Duane and Kruger's (*op. cit.*) results show that this period of high heat flow and hydrothermal activity was not limited to the Bushveld Complex, but co-existed with a period of hydrothermal activity covering large parts of the Kaapvaal Craton.

6.3 A Cratonic perspective on the intrusion of the Bushveld Complex

When measured up against other intrusive complexes, the B veld is enormous, wever, it forms only a small part of the Kaapvaal Craton. H ever, its effect, or ther an effect contemporaneous with its intrusion is felt on a aton wide scale. Duane & Kruger (*op. cit.*) have presente model for the dev ment of the Kaapvaal Craton during this period, the most significant feature being the Kheis orogeny in the western portion of the craton. The subduction of a lithospheric plate from a westerly direction explain many of the features seen at around this period. Subduction would supply the amount of heat required for all of these processes, and the fluids related to the subduction and orogeny could easily be driven by the heat for long distances, producing the alteration effects that are seen throughout the Kaapvaal Craton. The subduction and melting of a lithospheric plate would also provide a source for the crustal contamination of the Bushveld melt, evidenced in its high initial $^{87}Sr/^{86}Sr$ ratio, and crustal oxygen isotopic signature (pers. comm. F.J. Kruger).

7. The thermal event which gave rise to the formation of the Bushveld Complex continued after this final stage, its events still being detected as late as 1850 Ma ago (Allsopp *et al.*,1991; Walraven *et al.*,1990).

These stages in the development of the Bushveld Complex are summarised on Figure 6.1. It can be seen that a rough decrease in temperature can be traced from the intrusion through the end of the development of micas in the contact aureole, 13Ma later at a temperature of 586°C and the closure of the micas with respect to the Rb-Sr system, 31Ma later at a temperature of ±400°C to the final closure of the ^{40}Ar-^{39}Ar geochronometer 44 Ma later at a temperature of ±300°C. The immediate post-emplacement alteration of the rocks has led to the slightly low ages recorded using the Rb-Sr technique on micas and the wide spread of mica model ages.

This long cooling period, and long lasting alteration event indicate a far larger heating event than simply the intrusion of a large igneous complex , and confirms that the intrusion of the Bushveld and related complexes formed part of a craton wide tectono-thermal event in the time period 2.1-1.8 Ga.

6.2 The temporal and areal extent of the Bushveld Complex magmatism

This period spans 300Ma of the history of the Kaapvaal Craton, encompassing *inter alia* the Bushveld Magmatic Province and Phalaborwa Complex magmatism, the Vredefort event and the deposition of the Waterberg sediments. Bushveld magmas were intruded over a far wider area than the Bushveld Complex itself. Mafic Complexes such as the Losberg Complex are indistinguishable from the Bushveld Complex (Coetzee & Kruger, *op. cit.*), and a large number of dykes and sills are also found to be related to the Bushveld Complex. Metamorphic effects of this age are also seen far beyond the immediate contact aureole of the Bushveld Complex. Reset ages of 1.9-2.1 Ga have been determined throughout the Kaapvaal Craton (Duane & Kruger, 1990), and even onto the adjoining Zimbabwe Craton.

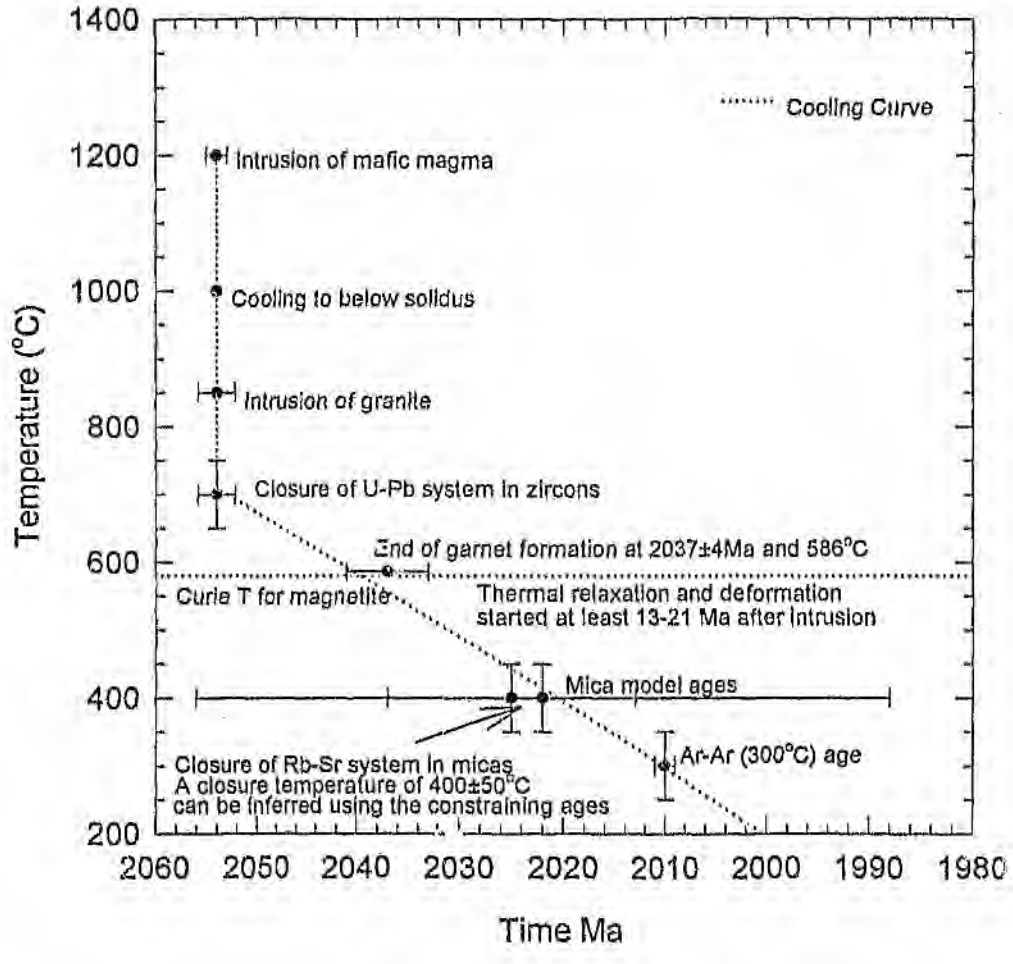

Figure 6.1 Cooling curve for the Bushveld Complex, illustrating the incremental development of the Complex, within a tectono-thermal framework.

rocks. Field relationships between the rocks indicate that the intrusion of the granite post-dates that of the mafic rocks. The geochronological results show however that the entire intrusion took place between 2056 and 2052 Ma.

4. After solidification the rocks continued to cool. The temperature remained at elevated levels for some time after the intrusion. The garnet Rb-Sr and geothermometric studies suggest a period of approximately 13 Ma to cool to a temperature of *c.* 586° C. This is very close to the Curie Temperature for magnetite (580° C), and is a significant result as Hattingh (1986a,b,c) has shown from palaeomagnetic data that the Bushveld Complex cooled to below the Curie Temperature before contraction and thermal relaxation resulted in the tilting of the rocks that we see today.

5. During this period of elevated temperature, Rb and Sr will have been relatively mobile in the micas in the mafic rocks. Even after the closure with respect to Rb and common Sr, radiogenic ^{87}Sr in the Rb sites in the micas may have remained mobile, the Sr ion being considerably smaller than the Rb ion, the site of which it occupied. Hydrothermal alteration of the micas was able to continually redistribute this $^{87}Sr^*$ within individual mica grains, resulting in a system with a wide variation in apparent ages between portions of grains, and an average model age approximating the age of final closure of the Rb-Sr system. This age is a further indication of the pervasive hydrothermal alteration experienced by the Bushveld Complex in the early stages of its development.

6. The initial Ar isotopic ratio was finally was finally "frozen" into the rocks 2010 Ma ago, indicating that the intrusion remained at elevated temperatures for several tens of millions of years after intrusion.

CHAPTER SIX: THE TECTONO CHRONOLOGICAL EVOLUTION OF THE BUSHVELD COMPLEX.

6.1 Evolutionary Chronology of the Bushveld Complex

The Bushveld Complex is usually seen as a single large magmatic event, and for most purposes this view is adequate. Field relationships indicate that the Bushveld Granite is younger than the mafic rocks, but recent high precision geochronology has produced ages for these two intrusive phases 0-3 Ma apart, and indistinguishable from one another. Furthermore, the work of Coetzee and Kruger (1988), and Barton (quoted in Walraven *et al.* (1990)) shows that the Losberg and Molopo Farms Complexes are probably also part of this magmatic event. These have been grouped together by Coetzee and Kruger (*op. cit.*) as the Bushveld Magmatic Province.

In addition to these related mafic intrusive rocks, the Phalaborwa Complex and the Vredefort structure were emplaced at about the same time and a pervasive metamorphic overprint is seen throughout the Kaapvaal Craton, dated at *c.* 2.0-2.1 Ga.

The ages quoted in this study indicate a number of geochronological features.

1. The mafic intrusion occurred at 2054±1 Ma (Armstrong, pers. comm.). This age has been repeated with zircons from various levels of the Rustenburg Layered Suite, indicating a brief period of magmatism, during which all phases of the Layered Suite were emplaced.

2. Cooling of the mafic magma to below the solidus will have taken less than 1 Ma (Walraven (1981), Irvine (1970)).

3. High precision geochronology has indicated that the intrusion of the Bushveld Granite occurred at an age within error of that of the intrusion of the mafic

$$T = -\frac{2109}{\ln K - 0.782}$$
$$= -\frac{2109}{\ln(0.1877) - 0.782} \qquad (19)$$
$$= 859K$$
$$= 586°C$$

The 13-21 Ma time period calculated in the previous section therefore refers to the period between the intrusion of the Bushveld Complex and the closure of the garnet. The rocks surrounding the Bushveld Complex were therefore still at a highly elevated temperature (586°C) up to 21 Ma after the intrusion. This study of the contact aureole of the Bushveld Complex has therefore placed constraints on the immediate post-intrusion history of the Bushveld Complex.

It is of note that this temperature is approximately the Curie Point for magnetite. The palaeopoles for the Bushveld Complex determined by Layer *et al.* (1988.), Gough and van Niekerk (1959) and Hattingh (1986a,b,c) in their palaeomagnetic studies must therefore be seen as the palaeopoles at the time that the Bushveld Complex cooled to below the Curie Point. Long periods of heating to temperatures below the Curie Point can also reset remanently magnetised bodies. It is therefore possible that the palaeomagnetic information from the Bushveld Complex represents an even later date than previously considered. This result has important implications for the structural history of the Bushveld Complex. The work of Hattigh (1986a,b,c) indicates that the remanent magnetisation of the complex was imprinted with the rocks in an horizontal position, *i.e.* they were horizontal until after the end of garnet growth at a temperature of 586°C. This occurred after the intrusion of the granite. Therefore, the thermal relaxation and centripetal collapse will only have started more than 13 Ma after the intrusion, with all the rocks already in a solid state.

Plotting ln K against 10000/T, a straight line is produced, with the equation:

$$\ln K = -\frac{2109}{T} + 0.782$$

where: $$K = \frac{\left(\frac{Mg}{Fe}\right)_{garnet}}{\left(\frac{Mg}{Fe}\right)_{biotite}} \qquad (17)$$

The garnet contains inclusions of biotite, and has zones of extremely low Mn concentration. This technique is therefore ideally suited to these samples.

5.3.2 Results

A garnet - biotite pair, with a low Mn concentration in the garnet, close to the edge of the garnet grain was chosen to obtain a temperature of closure for the garnet. These two grains were analysed using an electron microprobe. The relevant analytical data for these two samples is given below.

Table 5.4 Fe and Mg concentrations for a garnet-biotite pair in garnet GM-1

Mineral	FeO (wt. %)	MgO (wt. %)
garnet	36.43	3.61
biotite	18.68	9.86

Using these values measured in the probe study and re-writing the equation we obtain the following:

$$K = \frac{(Mg/Fe)_{garnet}}{(Mg/Fe)_{biotite}} = \frac{3.61}{36.43} \div \frac{9.86}{18.68} = 0.1877 \qquad (18)$$

Christensen, J. N., Rosenfeld, J. L. and DePaolo, D. J., 1989, Rates of tectonometamorphic processes from rubidium and strontium isotopes in garnet: Science, 244 (4911), 1465-1469.

Clift, R. A., 1985, Isotopic dating in metamorphic belts: J. geol. Soc. London, 142, 97-110.

Coetzee, H. and Kruger, F. J., 1989, The geochronology, Sr- and Pb- isotope geochemistry of the Losberg Complex: S. Afr. J. Geol., 92(1), 37-4[illegible].

Daly, R. A., 1928, Bushveld Igneous Complex of the Transvaal: Bull. Geol. Soc. Am., 39, 703-768.

Davies, G. and Cawthorn, R. G., 1984, Mineralogical data on multiple intrusion in the Rustenburg Layered Suite of theBushveld Complex: Mineral. Mag., 48, 469-480-bushveld.

Duane, M. J. and Kruger, F. J., 1990, Geochronological evidence for tectonically driven brine migration during the early Proterozoic Kheis Orogeny of southern Africa: Geophys. Res. Lett., 18(5), 975-978.

Eglington, B.M. and Harmer, R.E., 1993, A review of the statistical principles of geochronometry: II. Additional concepts pertaining to radiogenic U-Pb studies: S. Afr. J. Geol., 96(1/2), 9-21.

Eriksson, S. C., 1984, Age of carbonatite and Phoscorite magmatism of the Phalaborwa Complex South Africa: Chem. Geol., 46(4), 291-299.

Faure, G, 1986, Principles of isotope geology, John Wiley and Sons, New York, 589pp.

Perry, J.M. and Spear, F.S., Experimental calibration of the partitioning of Fe and Mg between biotite and garnet: Contrib. Mineral. Petrol., 66(2), 113-117.

Gilletti, B. J., 1974, Studies in diffusion. I. Argon in phlogopite mica: in Hoffman, A.W.,Gilletti, B.J., Yoder, H.S. & Yund, R.A. (eds) Geochemical Transport & Kinetics. Carnegie Instn. Washington, D.C., 106-116.

Gough, D. I. and Van Niekerk, C. B., 1959, A study of the paleomagnetism in the Bushveld Complex: Phil. Mag., 4, 126-136-bushveld.

Hall, A. L., 1932, The Bushveld Igneous Complex of the Central Transvaal: Geol. Surv. S. Afr., Mem. 28, 560.

Hamilton, J., 1977, Sr isotope and trace element studies of the Great Dyke and Bushveld mafic phase and their relationship to early Proterozoic magma genesis in Southern Africa: J. Petrol., 18, 24-52.

Harrison, T. M. and McDougall, I., 1980, Investigation of an intrusive contact in NW Nelson, New Zealand. I. Thermal, chronological and isotopic constraints.: Geochim. cosmochim Acta, 44, 1985-2003.

Hattingh, P. J., 1986a, The palaeomagnetism of the Merensky Reef footwall rocks of the Bushveld Complex: Trans. Geol. Soc. S. Afr., 89(1), 1-8.

Hattingh, P. J., 1986b, The palaeomagnetism of the main zone in the Bushveld Complex: Earth Planet. Sci. Lett., 79(3-4), 441-452.

Hattingh, P. J., 1986c, The palaeomagnetism of the main zone of the eastern Bushveld Complex: Tectonophysics, 124(3-4), 271-295.

Hunter, D. R. and Hamilton, P. J., 1978, The Bushveld Complex, in Tarling D.H. (ed.), Evolution of the Earths Crust, Academic Press, London, 107-173.

Irvine, T. N., 1970, Heat transfer during the solidification of layered intrusions, I. Sheets and sills: Can. J. Earth. Sci., 7, 1031-1061.

Jäger, E., Niggli, E. and Wenk, E., 1967, Rb-Sr-Altersbestimmungen an Glimmern der Zentralalpen: Beitr. geol. Karte Schweiz, NF134,Bern, 67pp.

Keppie, J. D., Dallmeyer, R. D., Krogh, T. E. and Ayuso, M., 1993, Dating mineralization using several isotopic methods: an example from the South Mountain Batholith, Nova Scotia, Canada: Chem. Geol. (Isot. Geosci. Sect.), 103, 251-270.

Kober, B., 1986, Whole-grain evaporation for $^{207}Pb/^{206}Pb$-age-investigations on single zircons using a double-filament thermal ion source: Contrib. Mineral. Petrol., 93, 482-490.

Kober, B., 1987, Single-zircon evaporation combined with Pb+ emitter bedding for $^{207}Pb/^{206}Pb$-age investigations using thermal ion mass spectrometry, and implications for zirconology: Contrib. Mineral. Petrol., 96, 63-71.

Kruger, F. J., Cawthorn, R. G. and Walsh, K. L., 1987, Strontium isotopic evidence against magma mixing in the upper zone of the Bushveld Complex: The Canadian Mineralogist, 23 (part 2), 306.

Kruger, F. J. and Marsh, J. S., 1982, Significance of $^{87}Sr/^{86}Sr$ ratios in the Merensky Cyclic Unit of the Bushveld Complex: Nature, 298(5869), 53-55.

Kruger, F. J. and Smart, R., 1987, Diffusion of trace elements during bottom crystallisation of double-diffusive convection systems; the magnetite layers of the Bushveld Complex: J. Volc. Geotherm. Res., 34(1-2), 133-142.

Layer, P. W., Kroner, A., McWilliams, M., and Clauer, N., 1988, Regional magnetic overprinting of Witwatersrand sediments, South Africa: J. Geophys. Res., 93(3), 2191-2200.

Ludwig, K. R., 1990, ISOPLOT: a plotting and regression program for radiogenic-isotope data, for IBM-PC compatible computers. Version 2.03: U.S.G.S. Open-File Rept. 88-557, 42pp.

Manton, W. I., 1987, Separation of Pb from normal zircons by single bead ion exchange: preservation to B.P.I staff.

Meintzer, L.M., 1987, Preparation of hydrofluoric, hydrochloric and nitric acids at ultra-low lead levels: Anal. Chem., 44, 1712-1718.

Menge C 1874, Carl Mandt's reise im innern von Süd Afrika, 1862-1875. Cottbe. 252pp.

McCarthy, T. S. and Cawthorn, R. G., 1980, Changes in initial $^{87}Sr/^{86}Sr$ ratio during protracted fractionation in igneous complexes: J. Petrol, 21(2), 342-364.

Molengraaff, G. A. F., 1901, Geologie de la Kaapkolonie Suid-Afrikaine dit Transvaal: Bull. Soc. Géol de France, 4 Sér: Tome 1, 13-95.

Moore, L. J., Moody, J. B., Barnes, I. L., Cramich, J. W., Murphy, T. J., Paulsen, P. J. and Shields, W. R., 1973, Trace determination of palladium and strontium in silicate glass standard reference materials: Anal. Chem., 45, 2384-2387.

Nicolaysen, L. O., De Villiers, J. W. L., Burger, A. J. and Strelow, F. W. E., 1958, New measurements relating to the absolute age of the Bushveld Igneous Complex: Trans. Geol. Soc. S. Afr., 61, 137-163.

O'Neill, J. R., Reimold, W. U. and Nicolaysen, L. O., 1987, Reconnaissance determinations of oxygen and hydrogen isotopic compositions of selected rocks from the Witwatersrand basin and Vredefort structure; South Africa: Contributions to the International Work,4pp.

Parrish, R. R., 1990, U-Pb dating on monazite and its application to geological problems: Can. J. Earth Sci., 27, 1431-1450.

Purdy, J. W. and Jäger, E., 1976, K-Ar ages on rock-forming minerals from the Central Alps: Mem. Ist. geol. mineral. Univ. Padova, 30, 1-31.

Sandberg, C. G. S., 1926, Or the probable origin of the members of the Bushveld Igneous Complex (Transvaal): Geol Mag, 63, 210-219.

Schiffries, C. M. and Skinner, B. J., 1987, The Bushveld hydrothermal system field and petrologic evidence: Amer J. Sci., 287, 566-595-bushveld.

Schreiner, G. D. L., 1958, Comparison of the ^{87}Rb-^{87}Sr ages of the red granite of the Bushveld Complex from measurements on the total rock and separated mineral fractions: Proc. Roy. Soc. Lond., Ser A 245, 115-117.

Sharpe, M. R., 1985, Strontium isotope evidence for preserved density stratification in the Main Zone of the Bushveld Complex: Nature, 316, 119-126.

South African Committee for Stratigraphy (SACS), 1980, Stratigraphy of South Africa, Part 1: Lithostratigraphy of the Republic of South Africa, South West Africa/Namibia and the Republics of Bophuthatswana, Transkei and Venda, Geological Survey of South Africa, Pretoria, 690pp.

Steiger, R. H. and Jäger, E., 1977, Subcommission on geochronology: Convention on the use of decay constants in geo- and cosmochronology: Earth Planet Sci. Lett., 36, 359-362.

Turner, D. L. and Forbes, R. B., 1976, K-Ar studies in deep basement drill holes: a new geologic estimate of Ar blocking in biotite (abstr): Eos, 57, 353.

van Biljon, S., 1949, The transformation of the Pretoria Series in the Bushveld Complex: Trans. Geol. Soc. S. Afr., 52, 1-175.

van Biljon, S., 1974, Transformation and deformation of the Pretoria Series in the south-western part of the Bushveld Complex: Trans. Geol. Soc. S. Afr., 77, 17-29.

von Gruenewaldt, G and Harmer, R.E., 1992, Tectonic setting of proterozoic layered intrusions with special reference to the Bushveld Complex: in Condie, K.C. (ed.) Proterozoic Crustal Evolution, Developments in Precambrian Geology, 10, 181-213.

Wagner, G. A., Reimer, G. M. and Jäger, E., 1977, Cooling ages derived by apatite fission track, mica Rb-Sr and K-Ar dating: the uplift and cooling history of the Central Alps: Mem. Ist. geol. Petrol. Univ. Padova, 30, 1-27.

Wagner, P. A., 1929, The pl. inum deposits and mines of South Africa: Oliver and Boyd, Edinburgh,326pp.

Walraven, F., 1981, Heat-transfer modelling in relation to the origin of the granophyre of the Bushveld Complex: Ann. Geol. Surv. S. Afr., 15(1), 33-48.

Walraven, F., Armstrong, R. A. and Kruger, F. J., 1990, A chronostratigraphic framework for the north-central Kaapvaal Craton, the Bushveld Complex and the Vredefort Structure: Tectonophysics, 171(1-4), 23-43.

Walraven, F, Smith, C.B. and Kruger, F.J., 1991, Age determinations of the Zoetlief Group: a Venterstorp Supergroup correlative: S. Afr. J. Geol., 94(2-3), 220-227.

Walraven, F. and Hattingh, E., 1993, Geochronology of the Nebo Granite, Bushveld Complex: S. Afr. J. Geol., 96(1-2), 31-41.

Wehring, M, 1981, Minimum curvature gridding routine, USGS Open File Report 1224, Fortran computer code.

Weis, D. and Wasserburg, G. J., 1987, Rb-Sr and Sm-Nd geochemistry and chronology of cherts from the Onverwacht Group (3.5AE), South Africa: Geochim. Cosmochim. Acta, 51, 973-984.

Wetherill, G. W., 1956, Discordant uranium-lead ages: Trans. Am. Geophys. Un., 37, 320-326.

Wright, C. J., McCarthy, T. S. and Cawthorn, R. G., 1983, Numerical modelling of trace element fractionation during diffusion controlled crystallisation: Computers and Geosciences, 9(3), 367-389.

York, D., 1969, Least squares fitting of a straight line with correlated errors: Earth Planet. Sci. Lett., 5, 320-324

Zykov, S. I. and Stupnikova, N. I., 1957: Isotopic analysis of lead not requiring any preliminary chemical preparation of the mineral, Geochem. Int, 506.